Simulation of Heat and Water Flow In Soil Under High Temperature (Fire) Conditions

June 1992

Coop Agreement Washington State University

FINAL REPORT FOR RESEARCH JOINT VENTURE AGMT
#INT-89448-RJVA with
WASHINGTON STATE UNIVERSITY
FS Contact: Roger Hungerford
Co-op Contact: Dr. Gaylon Campbell

Simulation of Heat and Water Flow in Soil Under High Temperature (Fire) Conditions

G. S. Campbell, J. D. Jungbauer, Jr.,
K. L. Bristow, and W. R. Bidlake
Dept. of Agronomy and Soils
Washington State University
Pullman, WA 99164

A report prepared for USDA, Forest Service, Intermountain Research Station, Intermountain Fire Sciences Lab., P. O. Box 8089, Missoula, MT 59807.

Jan. 1992

Overview

The objective of this project was to produce a simulation model capable of predicting soil temperatures and water contents under fire conditions. This involved not only producing a numerical model, but also testing the model and determining the thermal and hydraulic properties of soils and organic materials which would be needed to run the model for a range of conditions. This report presents the results of model development and testing, and the measurements and models of soil properties for a range of mineral and organic materials.

The report is presented in the form of several papers, each covering part of the work. The first paper describes the simulation model, the measurements made on heated soil columns, and the corroboration of the model using the measurements. Some model predictions for soil temperatures under natural fires are also presented. The second paper gives a detailed model of soil thermal conductivity at high temperatures, and presents a set of measurements on nine soils and peat moss which were used to derive model parameters and compare model performance to measurements. A third paper presents a new equation for predicting the water content-humidity relationship for soils, compares measurements with predictions, and tells how to estimate the parameters needed for this equation from texture or air dry water content measurements. The fourth paper presents results of thermal conductivity measurements on duff layers collected from the field. The final, short papers summarize several short experiments which were done to provide boundary condition information for the model, or corroborate other measurements.

In general, both the modeling and the measurement effort were very successful. With the information which we now have, we should be able to predict soil temperatures reliably, whatever the moisture, density, or mineralogy of the soil might be.

Soil Temperature and Water Content under Simulated Fire Conditions

G. S. Campbell, J. D Jungbauer, Jr., K. L. Bristow, and R. D. Hungerford

Introduction

When biomass on or above a soil surface burns, a heat pulse penetrates the soil. The resulting high soil temperatures can alter soil properties and kill roots, seeds and soil microbes. Since burning is often used as a management tool by foresters and range managers, it is important to know what soil and fuel conditions will be least detrimental to biological and physical properties. These conditions can be determined through experimentation, but experiments are expensive and difficult to conduct, and numerous physical factors affect the temperatures reached at different soil depths. A more economical approach is to use simulation models which explicitly account for the factors affecting soil heating.

A relatively complete model of heat and water movement under fire conditions was derived by Aston and Gill (1976) which included both liquid and vapor movement. While the results presented by Aston and Gill show reasonably good agreement with experiments for the soil they used, we have been far less successful in using the model with other soils and boundary conditions. Many of the relationships used by Aston and Gill are highly empirical and are based only on low temperature data. Also, the method for computing evaporation at high temperature is arbitrary, and the numerical techniques used are not stable for the highly non-linear differential equations needed to solve the soil heating problem.

The purpose of this paper is to present a model, based on equations similar to those used by Aston and Gill, but with improved descriptions of physical properties and improved numerical methods. Results of model simulations will be compared with measurements of temperature and water content from a heated laboratory column.

Transport Equations

When heat moves in a porous material, the total heat flux density (W m^{-2}), in one dimension, is given by the Fourier law:

$$J_h = -\lambda \, dT/dz \qquad (1)$$

where λ (W m^{-1} K^{-1}) is the apparent thermal conductivity of the soil (combined

sensible and latent transport), and dT/dz (K m^{-1}) is the temperature gradient. Conservation of energy requires that the change in heat storage at a point equal the divergence of the heat flux density, so

$$C_h \, \partial T/\partial t + H_v \, \partial J_v/\partial z = -\partial J_h/\partial z \qquad (2)$$

where C_h is the volumetric specific heat of the porous material (J m^{-3} K^{-1}), H_v (J kg^{-1}) is the latent heat of vaporization of water, and J_v (kg m^{-2} s^{-1}) is the vapor flux density. We will assume that, over the period of interest in fire simulation, liquid water flow is negligible, and that all changes in water content in the soil are from vapor transport so that

$$\rho_w \, \partial x_w/\partial t = -\partial J_v/\partial z \quad . \qquad (3)$$

where x_w (m^3 m^{-3}) is volume fraction of soil water and ρ_w (kg m^{-3}) is the density of water. Combining eqs (1), (2) and (3) gives the equation for heat transport and storage:

$$C_h \, \partial T/\partial t - H_v \rho_w \, \partial x_w/\partial t = \partial(\lambda \, \partial T/\partial z)/\partial z \qquad (4)$$

The flux density of water vapor in the soil is given by (de Vries, 1950)

$$J_v = - K_v/(1-p/P) \, dp/dz \qquad (5)$$

where K_v (kg m^{-1} Pa^{-1} s^{-1}) is the vapor conductivity in soil, P (Pa) is atmospheric pressure and p (Pa) is the partial pressure of water vapor in the soil. The term $1/(1-p/P)$ is a mass flow factor, called the Stefan correction, which accounts for the increase in mass of gas at the evaporating surface and the consequent drift of the bulk gas phase away from the surface when evaporation occurs.

Conservation of mass, with negligible liquid flux, is expressed by eq. (3). Combining eqs. (3) and (5) gives the equation for water transport and storage:

$$\rho_w \, \partial x_w/\partial t = -\partial\{[K_v/(1-p/P)] \, \partial p/\partial z\}/\partial z \quad . \qquad (6)$$

The relationship between p and x_w is not unique, but depends on temperature. To properly account for this, we express p as the product of relative humidity, h, and saturation vapor pressure at soil temperature, p^*:

$$p = hp^* \quad . \qquad (7)$$

The humidity is directly related to the water potential of the soil by

$$h = exp(M_w \psi/R\Theta) \qquad (8)$$

where M_w is the molecular mass of water (0.018 kg mol^{-1}), ψ is the water potential (J kg^{-1}), R is the gas constant (8.31 J mol^{-1} K) and Θ is Kelvin

temperature. Campbell and Shiozawa (1990) found a simple linear relationship between water content and $ln(-\psi)$, which is adequate for the purposes of these simulations. Water content is obtained from:

$$x_w = x_{w1}[1-ln(-\psi)/ln(-\psi_o)] \quad . \tag{9}$$

Here, x_{w1} is the extrapolated value of the water content when ψ = -1 J/kg, and ψ_o is the water potential of oven dry soil (-10^6 J/kg). Using the water potential of air dry soil ($\cong$ -10^5 J/kg) in eq. (9), we can show that $x_{w1} \cong 6x_{wa}$, where x_{wa} is the water content of air dry soil. A measurement of the water content of air dry soil is therefore all that is required to relate humidity, water content, and water potential of a soil sample. Equation (9) fails, for some soils, at water potentials above -1500 J/kg, but this corresponds to humidities above 0.99 so the error in calculation of p (eq. 7) is negligible. The derivatives, with respect to ψ, of both h and x_w, are readily obtained from eqs. 8 and 9. These are used in the numerical procedure to solve for new water potentials and temperatures.

The saturation vapor pressure is a function only of temperature. The formula of Richards (1971) was used with a slight modification of coefficients to fit data over the full range needed for fire conditions. Richards equation is

$$p^* = 101325\ exp(t(13.3016+t(-2.042+t(0.26+2.69t)))) \tag{10}$$

where t = 1-373.15/Θ; Θ is the Kelvin temperature. The maximum difference between predictions of eq. (10) and handbook data to temperatures of 373 C is 0.3%. The slope of the saturation vapor pressure function, which is needed for the numerical procedures, is readily obtained from eq. (10) by differentiation.

The apparent thermal conductivity of the soil is strongly temperature and water content dependent. A model, modified from de Vries (1963) (see Campbell et al., this report, for a detailed description) was used to predict thermal conductivity. The model is based on the assumption that the thermal conductivity of any mixture can be expressed as the weighted sum of the thermal conductivities of the components of the mixture. If we consider soil to be a mixture of water, gas and mineral, having volume fractions, x_w, x_a and x_m, with thermal conductivities, λ_w, λ_a and λ_m, then the overall thermal conductivity of the soil can be expressed as

$$\lambda = \frac{k_w x_w \lambda_w + k_a x_a \lambda_a + k_m x_m \lambda_m}{k_w x_w + k_a x_a + k_m x_m} \quad (11)$$

The thermal conductivity of the gas phase, λ_a, is considered to be an apparent thermal conductivity, which is the sum of the actual conduction through the air, λ_a^o, and the latent heat of distillation across pores in the soil, λ_v. The variation of the latent heat term with temperature is the primary factor responsible for temperature dependence of thermal conductivity in soil. Calculation of λ_v is treated in detail in Campbell et al. (this report) as are calculations to determine the weighting factors, k_a, k_w and k_m.

The vapor conductivity for the soil is determined by the air filled porosity and tortuosity of the soil pores, and by temperature and pressure. The conductivity is related to diffusivity by

$$K_v = \alpha a \eta M_w D_v / R\Theta \quad (12)$$

where α is a tortuosity correction (= 0.66), a is air filled pore space (x_{ws}-x_w), D_v is the diffusivity for water vapor in air (m^2 s^{-1}), and η is a vapor flow enhancement factor (Philip and de Vries ,1957). The temperature and pressure dependence are introduced through (Fuller et al, 1966):

$$D_v = D_{vo}(P_o/P)(\Theta/\Theta_o)^{1.75} \quad (13)$$

where D_{vo} is the diffusivity at STP and the subscript o's indicate standard temperature and pressure. Philip and de Vries (1957) show that η is the product of two factors, one arising from liquid movement across pores assisting in vapor transport, and one from the ratio of microscopic (within pore) temperature gradients to macroscopic gradients. The first term is unity for dry soil and around 3 when soil is wet. The second term is equal to the weighting factor, k_a in eq. 11.

Numerical Implementation

Computer code to implement the model was written in Turbo Pascal. The code is included in the appendix of this report. The model uses specified initial and boundary conditions and soil property data to predict temperature and water content in a soil column which is heated strongly at the surface. Surface boundary conditions are a specified air temperature and vapor pressure, and a specified radiant energy input at the soil surface. Generally

about thirteen nodes were used for a simulation, with node spacings of 5 mm or less near the surface and increasing spacings at deeper depths. The bottom node was generally at 95 mm and was set to measured temperature or water content conditions. A time step of 30 s. was used for most simulations, but was decreased to 10 s in one case where rapid heating at the surface caused the solution not to converge.

After setting up initial conditions and model parameters, the program sets top and bottom boundary conditions, and then solves, simultaneously, for new temperatures and water potentials. New humidities and water contents are computed from the water potentials. Versions of the model were written with water content and with humidity as the primary water variable, in addition to the version described here where water potential is the primary variable. The version with potential is much faster and more reliable because it avoids numerical problems when soils are wet or extremely dry.

A Newton-Raphson (iterative) numerical method (Campbell, 1985) is used to simultaneously solve the highly non-linear difference equations for both temperature and water content. The full Newton-Raphson procedure requires that we find, with each iteration, values of $\Delta\psi$ and ΔT for each node which will reduce the mass or heat balance error for that node. Iteration continues until the node values of ψ and T give mass and heat balance within a specified error. For any node, i, the equations to solve for $\Delta\psi_i$ and ΔT_i are

$$\sum_{k=i-1}^{i+1}\left[\frac{\partial H_i}{\partial T_k}\,\Delta T_{ki} + \frac{\partial H_i}{\partial \psi_k}\,\Delta \psi_{ki}\right] = H_i \qquad (14a)$$

and

$$\sum_{k=i-1}^{i+1}\left[\frac{\partial W_i}{\partial T_k}\,\Delta T_{ki} + \frac{\partial W_i}{\partial \psi_k}\,\Delta \psi_{ki}\right] = W_i \qquad (14b)$$

Here, H_i and W_i are the mass balance errors for heat and water at node i. These are calculated from the discretized forms of eqs. (4) and (6):

$$H_i = K_{i-1}(T_i-T_{i-1})-K_i(T_{i+1}-T_i)+(\Delta z_i/\Delta t)[C_h(T_i^{j+1}-T_i^j)-\rho_w H_v(x_{wi}^{j+1}-x_{wi}^j)] \qquad (15)$$

and

$$W_i = G_{i-1}(p_i-p_{i-1})-G_i(p_{i+1}-p_i)+(\Delta z_i/\Delta t)[\rho_w(x_{wi}^{j+1}-x_{wi}^j)] \qquad (16)$$

The element conductances, G and K, are averages of the conductivities for

vapor or heat of the nodes at each end of the element, divided by the element length. The superscript, j, indicates the value at the beginning of the time step, and j+1 is the value at the end.

Normally, eqs. (14) are written for each node and solved simultaneously for the $\Delta\psi_i$ and ΔT_i. This requires inversion of a matrix of bandwidth 6. While this is not difficult, we used another approach which requires less computer memory, and often less time in iterative problems like this one. Our simple method uses only the derivatives with respect to node i, and therefore allows solution of one node at a time. The equations to solve are:

$$\frac{\partial H_i}{\partial T_k}\Delta T_{ki} + \frac{\partial H_i}{\partial \psi_k}\Delta \psi_{ki} = H_i \tag{17}$$

$$\frac{\partial W_i}{\partial T_k}\Delta T_{ki} + \frac{\partial W_i}{\partial \psi_k}\Delta \psi_{ki} = W_i \tag{18}$$

Equations (15) and (16) both depend on temperature and water content, and all four derivatives are readily calculated using the equations given previously and the chain rule of calculus. Once the mass balance errors and the derivatives are known, eqs. (17) and (18) are readily solved for the new estimates of temperature and water potential. These are used to update the estimates of water content, humidity, vapor pressure and conductivity, and, if the heat or mass balance error is larger than a specified tolerance, the iteration is repeated.

The vapor surface pressure, temperature, and radiant flux density are assumed to increase toward a final value, V_f according to $V = V_f[1\text{-}exp(t/\tau)]$, where τ is a time constant which depends on the heater used for the simulation. The final temperature, vapor pressure and radiant flux densities were either measured or estimated for each simulation. Radiant flux density from the soil surface was computed using the Stefan-Boltzman law with an emissivity of 0.9. The heat and mass transfer coefficients for the soil surface were set at 20 W $m^{-2}K^{-1}$ and 1.24 x 10^{-7} kg m^{-2} Pa^{-1}. We were not able to obtain precise values for these variables through measurement, but found that the model is insensitive to the exact values chosen.

The Stefan correction, shown in eq. (5), approaches infinity as the water approaches boiling temperature. In order to avoid numerical problems from this, it was necessary to constrain the correction to be > 0.3. A small correction was added to the thermal and vapor conductances to account for effects of convection. The convection correction was directly proportional to the rate of vapor production at nodes lower in the profile.

Materials and Methods

The experimental setup used for monitoring heat and water flow is shown in Figure 1. The soil column was packed into a cylindrical container 12 cm in diameter and 15.5 cm high made from a coffee can. This container was fastened at the bottom in the center of a larger coffee can 15 cm in diameter and 17.5 cm high. The space between the two cans was filled with glass wool to insulate the inner can from direct heating of the metal, and to cover the path of thermocouple wires which ran through the sides of the inner can and out through a hole in the middle of the outer can. Copper-constantan thermocouples were placed at the surface, at 10 mm depth increments from 5 mm to 35 mm below the soil surface, and at 30 mm increments from 35 to 95 mm deep. Each thermocouple was held within a piece of 1 mm diameter stainless steel tubing, 13 cm long, which ran across the can, supported in holes at the sides by small ceramic insulators. Soil temperature was measured at a junction in the center, and horizontal temperature differences were checked between the center junction and another approximately 4 cm toward one side on the same level.

The soil was mixed separately to the desired water content, sealed in plastic, and allowed to equilibrate. It was then packed into the can, to the top, and the entire assembly was weighed, in order to calculate bulk density.

Changes in water content were measured by gamma ray attenuation using a collimated 500 mCi ^{137}Cs source (Gardner et al., 1972). The packed can assembly was placed on a platform between the Cesium source and a NaI detector. Both the source and the detector were collimated to a 5 mm diameter beam. The gamma beam ran through a diameter of the can perpendicular to the thermocouples.

The soil column was heated using a propane-fired infrared portable construction heater (model MH14TC, Mr. Heater Corp., Cleveland, OH). The

heated element was approximately 10 cm in diameter, and was surrounded by a reflector and heat shield which was 22 cm diameter. The heater was placed 35 mm above the soil surface. The radiant flux density at the soil surface was measured using a water-cooled radiometer (Campbell, this report). Two heater settings were used. On high, the radiant flux density was 54 kW m^{-2}, and on the low setting it was 39 kW m^{-2}.

An IBM PC compatible microcomputer with a counter-timer expansion board (model CTM-05, MetraByte Corp., Taunton, MA) was used to count the gamma radiation and control a motorized table which positioned the soil column in the gamma beam. The column was scanned at 9 levels: every 5 mm from 5 mm to 35 mm; then every 30 mm down to 95 mm deep. An initial scan with no heating was made for 50 seconds at each level in order to accurately determine the initial gamma counts. When heating began, the platform cycled from top to bottom through all 9 levels, stopping at each level to count for 10 seconds. A microprocessor-controlled data logger (model CR7X, Campbell Scientific, Inc., Logan, UT 84321) was also controlled by the microcomputer, and recorded temperature from a thermocouple as the water content for that depth was being measured. Each cycle, including the return of the can to its initial position, lasted just under 2 minutes. Data collection continued until the top 3 levels had exceeded 100°C.

Changes in water content were calculated using the following formula derived from equation [43] of Gardner (1986):

$$\Delta\theta = -\ln(I_t/I_o)/\mu_w S$$

where $\Delta\theta$ is the change from the initial time to time t in the mass of water per unit bulk volume of soil, I_t is the gamma count rate at time t, I_o is the count rate at the initial time, μ_w is the mass attenuation coefficient for water, and S is the thickness of the soil column. This formula assumes a constant bulk density over time. For each time interval and soil depth, water content was calculated from these changes with reference to the initial water content at which the soil was mixed.

Samples of four soils were used: Quincy sand, Bouldercreek silt loam, the high-clay B horizon of a Palouse soil, and Volkmar silt loam. Quincy sand is from the Hanford nuclear reservation in Central Washington, and is classified as mixed mesic Xeric Torripsamments. Palouse is a fine-silty, mixed, mesic Pachic Ultic Haploxeroll from Whitman County, WA. Bouldercreek is a Medial

over loamy-skeletal, mixed frigid Typic vitrandepts taken from the mountains near Wallace, ID. It represents a large area of soils in Northern Idaho and Western Montana referred to as "ash cap" soils. Volcanic ash, thought to have come from the eruption of Mt. Mazama, is a dominant component of these soils, giving them a very low mineral thermal conductivity. The Volkmar soil is anAeric Cryaquept from Delta, Alaska. It was used because of its high mineral conductivity. Relevant properties for the simulations, for each soil, are given in Table 1.

Soils were dried to air dryness, passed through a 2 mm sieve, and stored for use in the heating experiments. Measurements were made only on the sieved portions, which were mixed to varying water contents as previously described. All water contents are reported on an oven dry (105°C) basis even though the water contents of samples under fire conditions can go much lower as the samples reach temperatures several hundred degrees above the standard oven temperature..

Results and Discussion

Results from the heating experiments are shown as the squares in Figs. 2-14. Consider first the Palouse soil in Fig. 2a. The temperature at each depth quickly rises to a value approaching the boiling temperature, and remains there until that layer is almost completely dry. The rapid warming of the moist soil is an indication of the high apparent thermal conductivity of moist soil at these temperatures. The almost constant temperature of the heated soil near 100 C results from the large quantity of latent heat required to evaporate the water from the soil. The water content in each layer (Fig. 2b) remains relatively constant, or rises slightly, and then decreases quickly to values near or below zero. The abrupt rise in layer temperature occurs when the water content of that layer drops below about 0.02 m^3 m^{-3}.

The constant temperature plateau reached by the moist soil is near the boiling point, but does not reach boiling temperature. In Fig. 2 the temperature of each layer remained constant at 96.5 C $\pm$ 0.5 C during the final portion of each plateau. Apparently the temperature rises and the mass flow factor (eq. 5) decreases until the rate of evaporation of water out of a layer just balances the rate of heat supply. The rate of heat supply

and the amount of water to be evaporated are therefore critical factors in determining the soil temperatures reached in any heating event.

Figure 3 shows temperatures and water contents for air dry Palouse soil. The pattern is similar to that with the moist soil, but the plateau is much shorter (because of the small amount of water in the soil) and surface temperatures increase much more quickly. Note, however, that heat transfer to lower levels in the soil is slower than for wet soil because of the low thermal conductivity of the dry soil and the absence of latent heat transfer.

Figure 6 shows temperatures in Quincy sand that was kiln-dried at 600 C before the run. Here there is no evidence of moisture effects. Water content changes (not shown) occurred only in the top layer that took up water from the atmosphere prior to application of heat.

A fairly consistent feature of the water content measurements is the negative water contents which obtain in the upper layers at high temperatures. Water contents are reported on an oven dry (105 C) basis, so additional water loss is expected at temperatures several hundred degrees above this value. It is likely, however, that some of the apparent change in gamma count, which we have interpreted as change in water content, results from volatilization of other soil constituents, or possibly heat induced changes in soil density. It is interesting, however, to note (for example Figs. 2b and 3b) that the water content of the underlying soil strongly affects the apparent water loss of the upper layers. In air dry soil, water contents below -0.07 Mg m^{-3} were observed in both the Boulder Creek and Palouse soils, while the upper layers of the wetter soils remained near zero during heating.

Simulation results are shown as the full lines in Figs. 2-14. It appears that the main features of both the heating and the drying are well simulated by the model for the wide range of soil textures, water contents, mineral thermal conductivities, and bulk densities present in the experiments. Sensitivity tests show the temperature simulations to always be within experimental uncertainty (of the independently measured model parameters and boundary conditions) of the measured values.

The water simulations show drying times which are generally in good agreement with measurements, but the time-course of water content changes is certainly different for measurements and simulations. The simulations consistently show a buildup of water ahead of the drying front, while the

measurements either do not show this effect, or show it to be very small. One version of the model (based on somewhat different mass flow assumptions) was able to match the measured drying curves more closely, but produced temperatures which were well below measured values. In other words, a drying rate which is consistent with the measured water contents produces a latent heat loss which is inconsistent with the temperature measurements. We do not know, therefore, whether the disagreement between the model and the measurements is the result of a failure in the model or the measurements. It is possible that liquid water flow plays a role. We did not include this in the model because of the substantial increase in complexity of such a model and the difficulty in getting reliable hydraulic parameters for soil at high temperature. Since our main interest is in predicting temperature, and the model consistently predicts correct soil temperatures in spite of uncertainties in the drying patterns, we felt it unnecessary to further complicate the model.

The model consistently predicts negative water contents in the strongly heated upper layers of the soil, but does not show a strong effect of initial water content on these values, as the data do. At this point we do not understand why water deeper in the soil affects the apparent water content of the upper layers so strongly, and therefore are not able to model the phenomenon. As with the moisture buildup ahead of the wetting front, however, it appears not to strongly affect our ability to predict soil temperatures.

Model Application

In order to provide some insight into possible effects of fire on chemical and biological systems in the soil, we used the model to simulate soil temperatures under several different fire conditions. Hungerford et al. (1991) show soil temperatures (2 cm depth) measured under grass, shrub and duff fires. We assumed these to have been measured in a typical silt loam soil at field capacity, and found upper boundary conditions for the model which gave 2 cm temperatures matching the published values. The depth of the bottom node was increased to 32 cm, and this temperature was held constant at 20 C. Simulations were then run with soil starting at field capacity and at air dryness, and the results were plotted to show isotherms in depth and time.

Figures 15-20 show the isotherms. Note that the depth scale is logarithmic to more clearly show the temperature distribution near the surface.

The duration of the fire plays a key role in the depth of penetration of the heat pulse. The 200 C isotherm penetrates only a few millimeters under the grass fire, but penetrates to perhaps 100 mm under the duff fire. The moisture effect is an interesting one. In general, temperatures above the boiling point go deeper in the dry soil than the wet, indicating that the vaporization of water tends to contain the heating front. On the other hand, the higher thermal conductivity of the wet soil transmits heat more readily at temperatures below the boiling point, so the isotherms below 100 C penetrate more deeply into the wet soil. It is somewhat surprising, however, that temperatures are as similar as they are between the two water levels.

Conclusions

Measurements of temperature and water content in a soil column which was heated strongly at the surface show a consistent pattern of warming and drying. When the soil is initially wet, temperature rises quickly to around 90 C and remains there until the water content of the soil at that depth drops below about 0.02 Mg m^{-3}. When the soil is dry, the temperature abruptly increases. Even the moisture present in air dry soil is sufficient to show this heating pattern. Water content may increase slightly ahead of the drying front, and then drops rapidly, generally to values below the standard, oven dry value. The lowest water contents reached depended on the initial water content of the soil. Air dry soil reached lower water contents in the heated layers than did initially moist soil.

A linked-transport model, which simultaneously computes changes in temperature and water content, appears to correctly simulate the main features of heat and water flow in a soil column heated to high temperature. There were no consistent deviations of measured from modeled temperatures, but the water content simulations consistently showed a greater buildup of moisture ahead of the heating front than did the measurements, and less drying of the soil in the heated layers when the initial soil water content was low. Soils from sand to clay, and with differing mineralogies, water contents, and bulk densities were used to compare measurements and simulations. The model performed well in all cases. Since the temperature simulations are

reasonable, the model appears suitable for use in predicting fire effects in the field.

Simulations were run using boundary conditions similar to those under grass, shrub, and duff fires in the field, and resulting isotherms with depth and time were produced.

References

Aston, A. R. and A. M. Gill. 1976. Coupled soil moisture, heat and water vapour transfers under simulated fire conditions. Aust. J. Soil Res. 14:55-66.

Campbell, G. S. 1985. Soil Physics with BASIC: Transport models for soil-plant systems. Elsevier, New York, 150 p.

Campbell, G. S., J. D. Jungbauer Jr., W. R. Bidlake and R. D. Hungerford. 1990. Predicting thermal conductivity of soil at high temperature. (part of this report)

Campbell, G. S. and S. Shiozawa. 1991. Prediction of hydraulic properties of soils using particle size distribution and bulk density data. Proceedings of a workshop: Indirect Methods of Estimating the Hydraulic Properties of Unsaturated Soils. U. S. Salinity Laboratory, Riverside, CA. in press.

de Vries, D. A. 1958. Simultaneous transfer of heat and moisture in porous media. Trans. Am. Geophys. Union 39:909-916.

de Vries, D. A. 1963. Thermal properties of soils. p. 210-235. In W. R. van Wijk (ed.) Physics of Plant Environment. North Holland Publ. Co., Amsterdam.

Gardner, W. H. 1986. Water Content. p. 493-543 in Methods of Soil Analysis, Part 1. Agronomy Monograph no. 9, American Society of Agronomy, Madison, WI.

Hungerford, R. D., M. G. Harrington, W. H. Frandsen, K. C. Ryan and G. J. Niehoff. 1991. Influence of fire on factors that affect site productivity. in Proceedings -- Management and Productivity of Western - Montane Forest Soils. USDA Forest Service, Intermountain Research Station General Technical Report INT-280, Missoula, MT.

Philip, J. R. and D. A. de Vries. 1957. Moisture movement in porous materials under temperature gradients. Trans. Am. Geophys. Union. 38:222-232.

Richards, J. M. 1971. Simple expression for the saturation vapor pressure of water in the range -50 to 140. Brit. J. Appl Phys. 4:L15-L18.

Table 1. Thermal and hydraulic properties of soils used for the simulations.

Soil	x_{w1} m^3m^{-3}	λ_m W/(mK)	x_{wo} m^3m^{-3}	g_a -	q_o -	ρ_m Mg/m^3
Quincy	0.064	2.61	0.091	0.090	3.01	2.82
Bouldercreek	0.32	1.03	0.133	0.130	6.08	2.13
Palouse B	0.37	2.00	0.230	0.074	5.83	2.65
Volkmar	0.055	4.71	0.150	0.116	1.71	2.65

Figure Captions

Figure 1. Experimental setup for measurement of water content and temperature under simulated fire conditions.

Figures 2 - 14. Measured (points) and modeled (lines) temperatures and water contents for soil columns heated at the surface with a propane burner.

Figure 15. Simulated isotherms showing temperature distributions under a grass fire with initial soil water content near field capacity. Depth is logarithmic.

Figure 16. Simulated isotherms showing temperature distributions under a grass fire with initial soil air dry. Depth is logarithmic.

Figure 17. Simulated isotherms showing temperature distributions under a shrub fire with initial soil water content near field capacity. Depth is logarithmic.

Figure 18. Simulated isotherms showing temperature distributions under a shrub fire with initial soil water content air dry. Depth is logarithmic.

Figure 19. Simulated isotherms showing temperature distributions under a duff fire with initial soil water content near field capacity. Depth is logarithmic.

Figure 20. Simulated isotherms showing temperature distributions under a duff fire with initial soil water content air dry. Depth is logarithmic.

Cross-section of can assembly

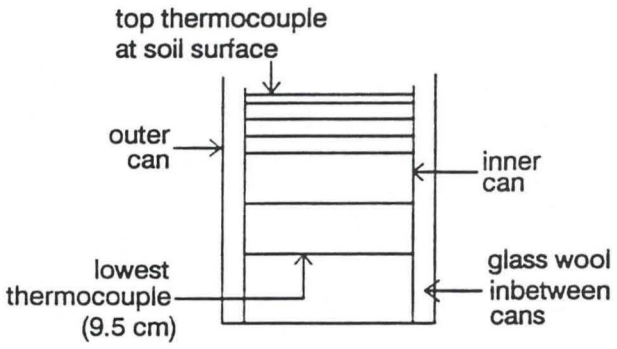

Gamma Equipment and General Layout

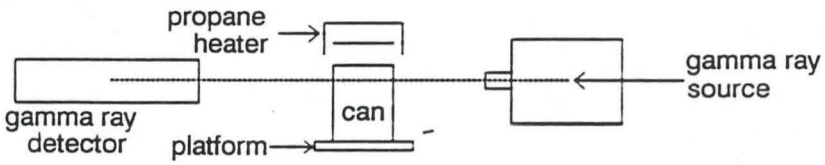

Fig 1

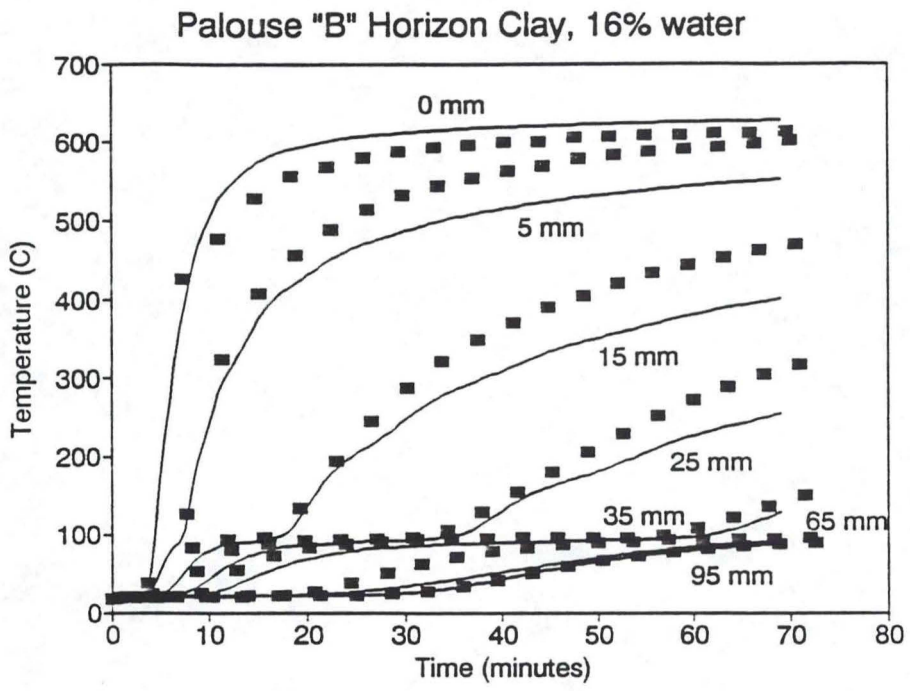
Palouse "B" Horizon Clay, 16% water
Temperature (C)
Time (minutes)
0 mm
5 mm
15 mm
25 mm
35 mm
65 mm
95 mm
0
100
200
300
400
500
600
700
0
10
20
30
40
50
60
70
80

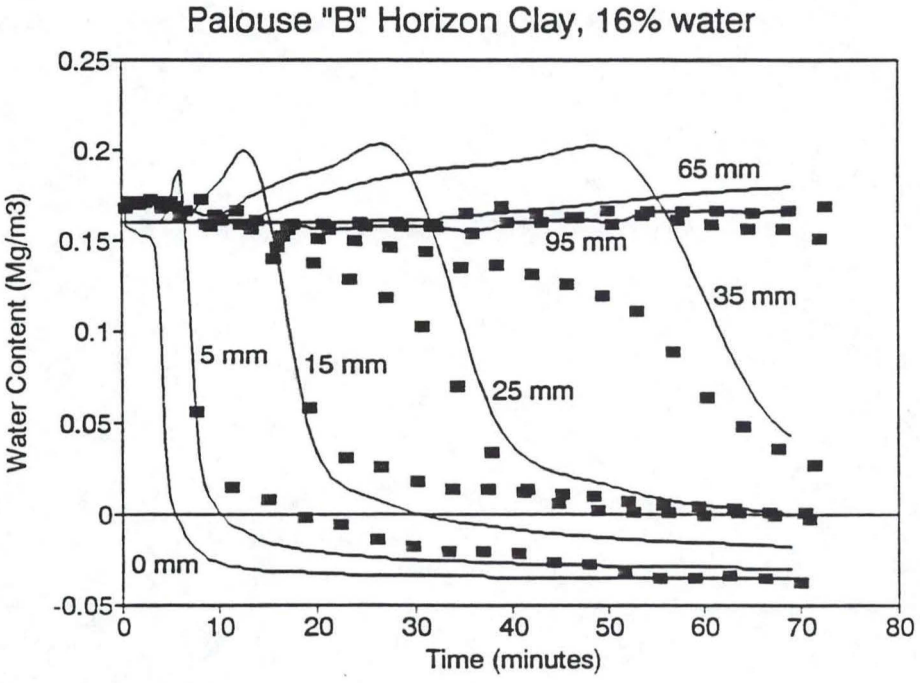
Palouse "B" Horizon Clay, 16% water
Water Content (Mg/m3)
Time (minutes)
65 mm
95 mm
35 mm
5 mm
15 mm
25 mm
0 mm
0.25
0.2
0.15
0.1
0.05
0
-0.05
0
10
20
30
40
50
60
70
80

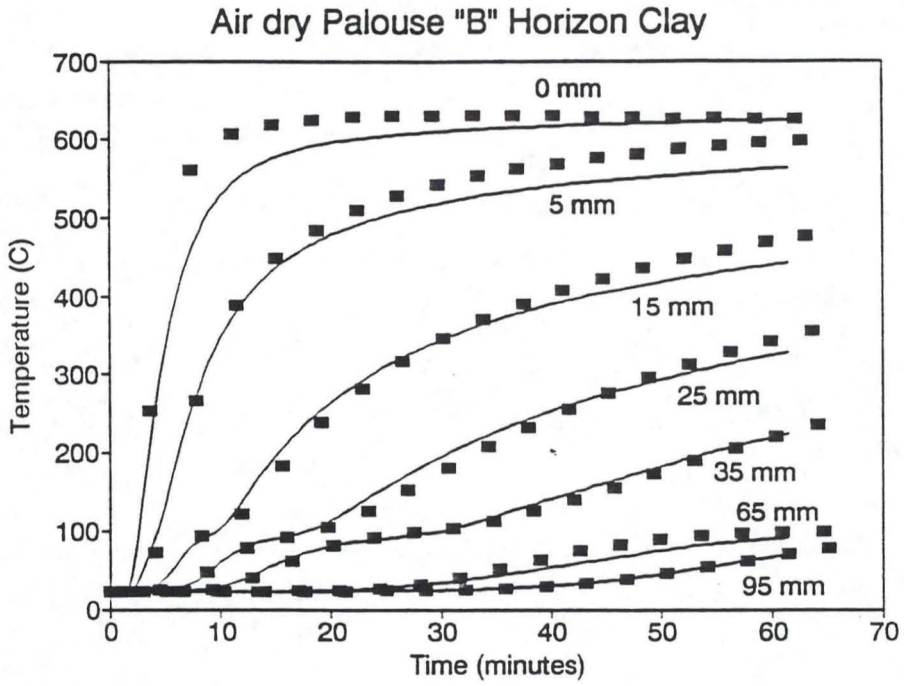
Air dry Palouse "B" Horizon Clay
Temperature (C)
Time (minutes)
0 mm
5 mm
15 mm
25 mm
35 mm
65 mm
95 mm
0
100
200
300
400
500
600
700
0
10
20
30
40
50
60
70

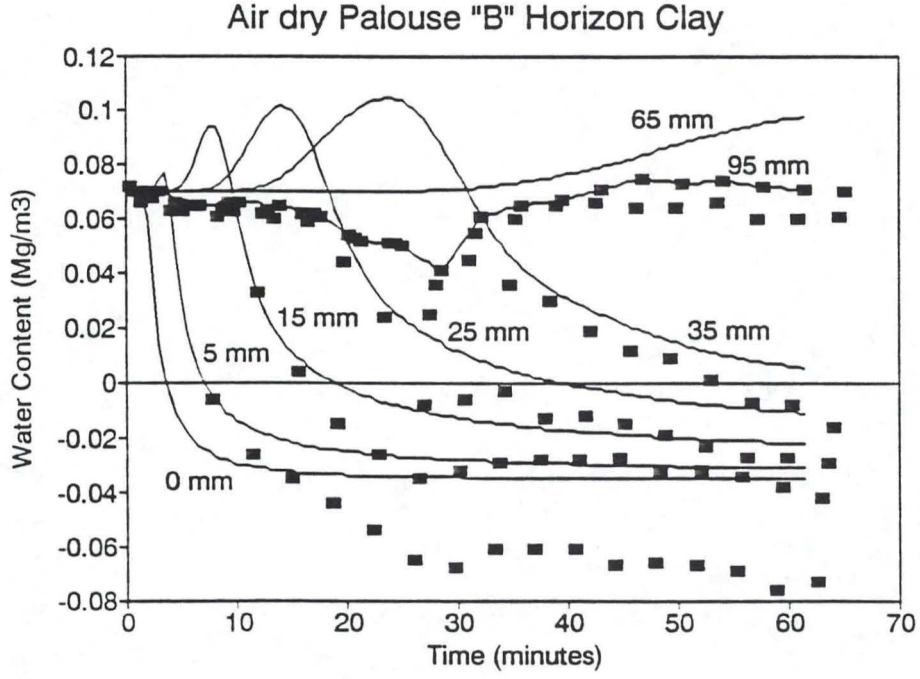
Air dry Palouse "B" Horizon Clay
Water Content (Mg/m3)
Time (minutes)
65 mm
95 mm
15 mm
25 mm
35 mm
5 mm
0 mm
0.12
0.1
0.08
0.06
0.04
0.02
0
-0.02
-0.04
-0.06
-0.08
0
10
20
30
40
50
60
70

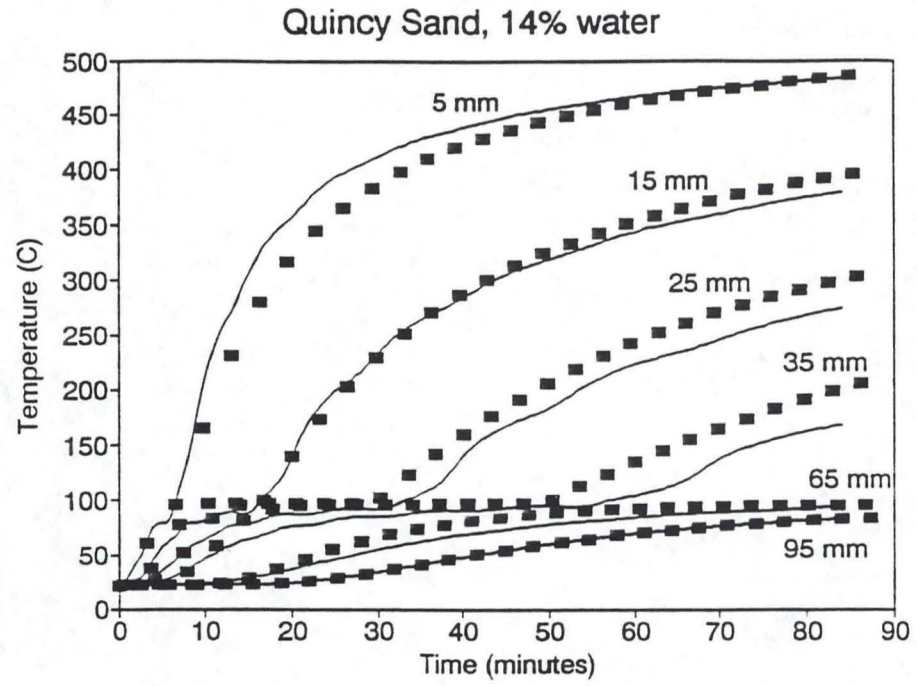
Quincy Sand, 14% water
Temperature (C)
Time (minutes)
5 mm
15 mm
25 mm
35 mm
65 mm
95 mm
0
50
100
150
200
250
300
350
400
450
500
0
10
20
30
40
50
60
70
80
90

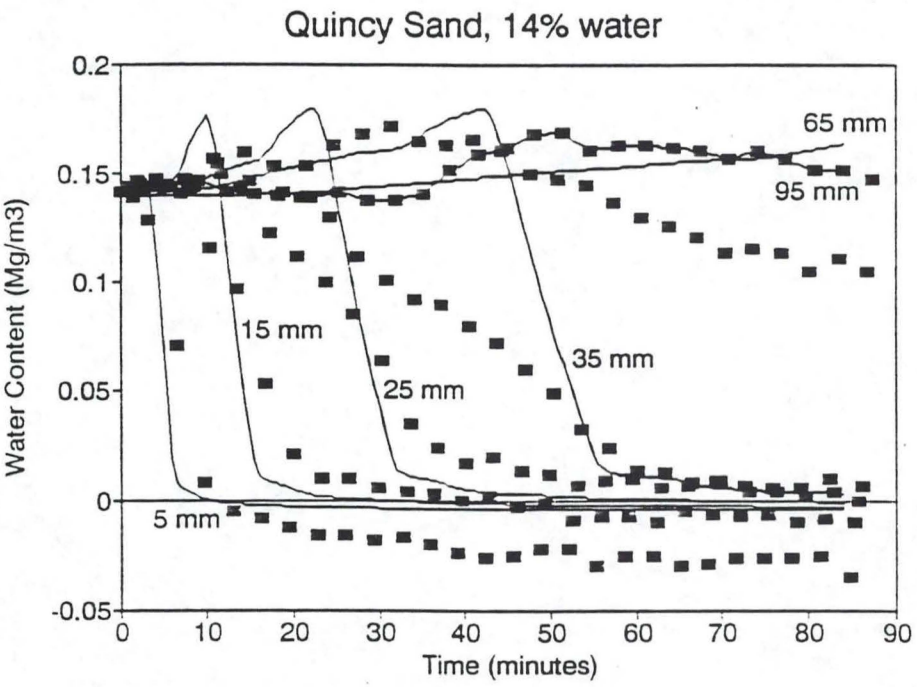
Quincy Sand, 14% water
Water Content (Mg/m3)
Time (minutes)
65 mm
95 mm
15 mm
35 mm
25 mm
5 mm
-0.05
0
0.05
0.1
0.15
0.2
0
10
20
30
40
50
60
70
80
90

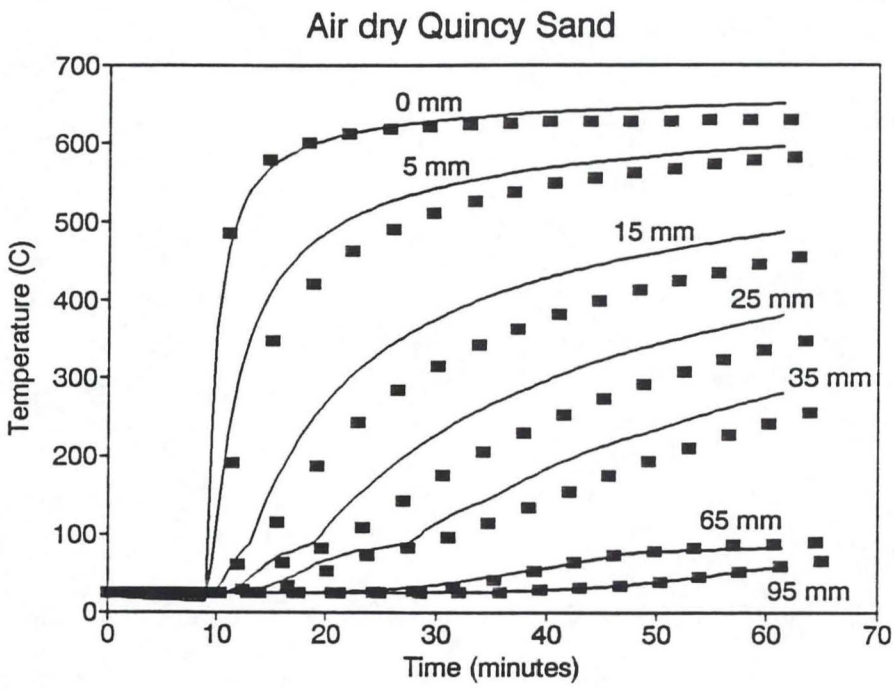
Air dry Quincy Sand
Temperature (C)
Time (minutes)
0 mm
5 mm
15 mm
25 mm
35 mm
65 mm
95 mm
0
100
200
300
400
500
600
700
0
10
20
30
40
50
60
70

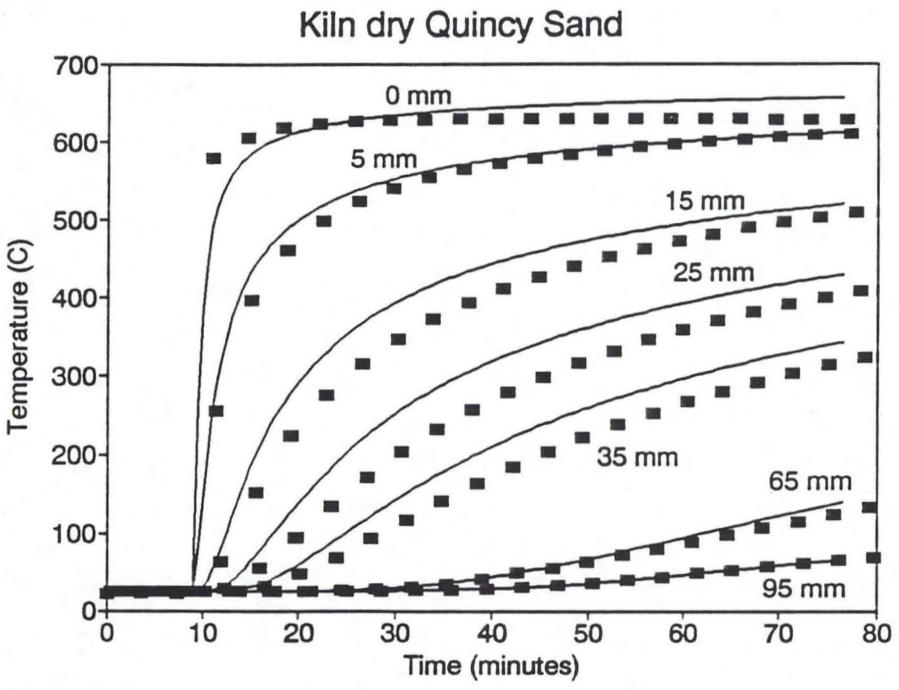
Kiln dry Quincy Sand
Temperature (C)
Time (minutes)
0 mm
5 mm
15 mm
25 mm
35 mm
65 mm
95 mm
0
100
200
300
400
500
600
700
0
10
20
30
40
50
60
70
80

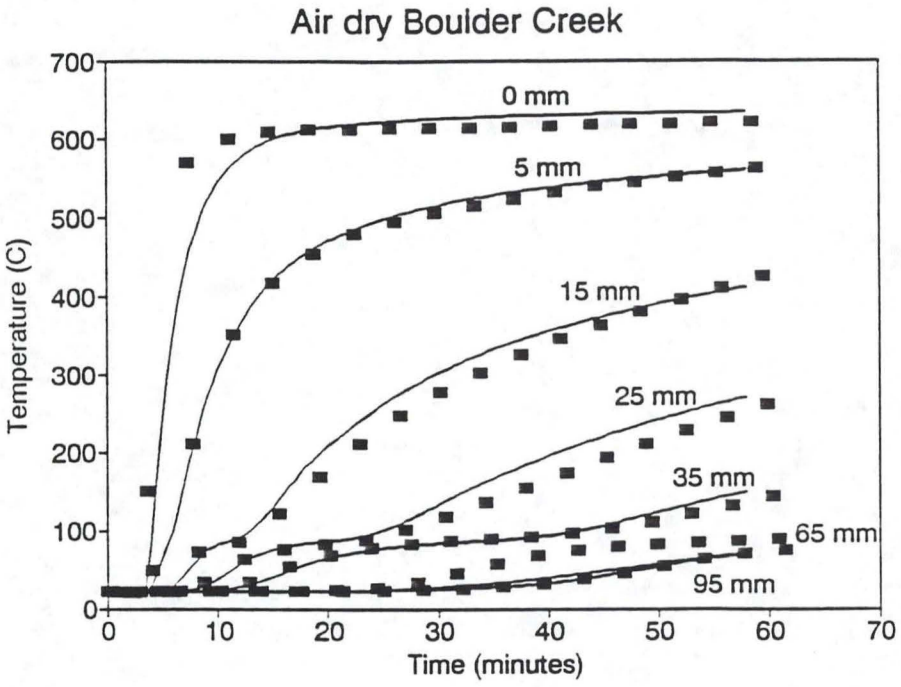
Air dry Boulder Creek
Temperature (C)
Time (minutes)
0 mm
5 mm
15 mm
25 mm
35 mm
65 mm
95 mm
700
600
500
400
300
200
100
0
0
10
20
30
40
50
60
70

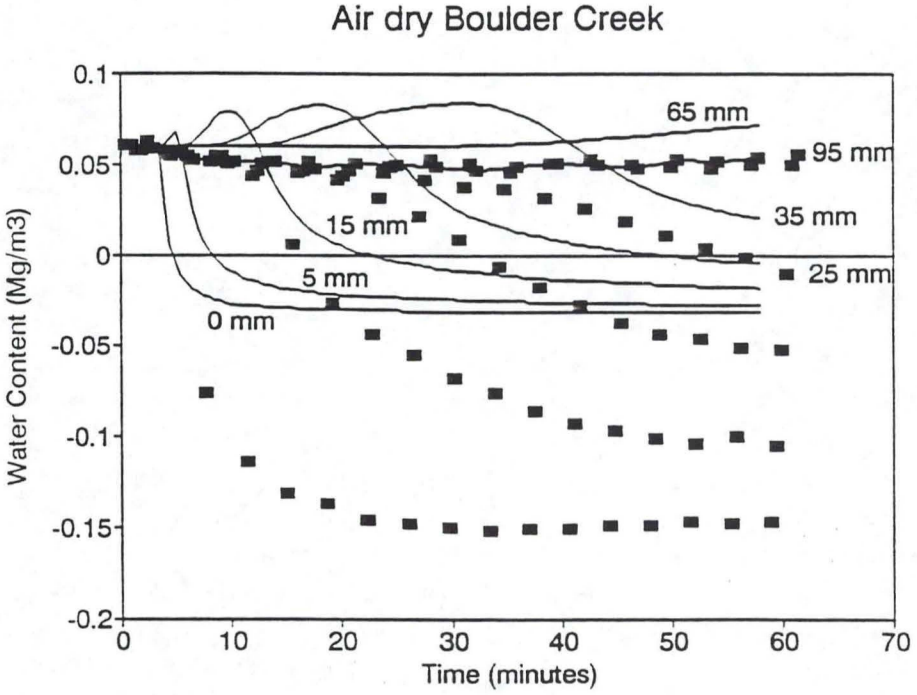
Air dry Boulder Creek
Water Content (Mg/m3)
Time (minutes)
65 mm
95 mm
35 mm
15 mm
25 mm
5 mm
0 mm
0.1
0.05
0
-0.05
-0.1
-0.15
-0.2
0
10
20
30
40
50
60
70

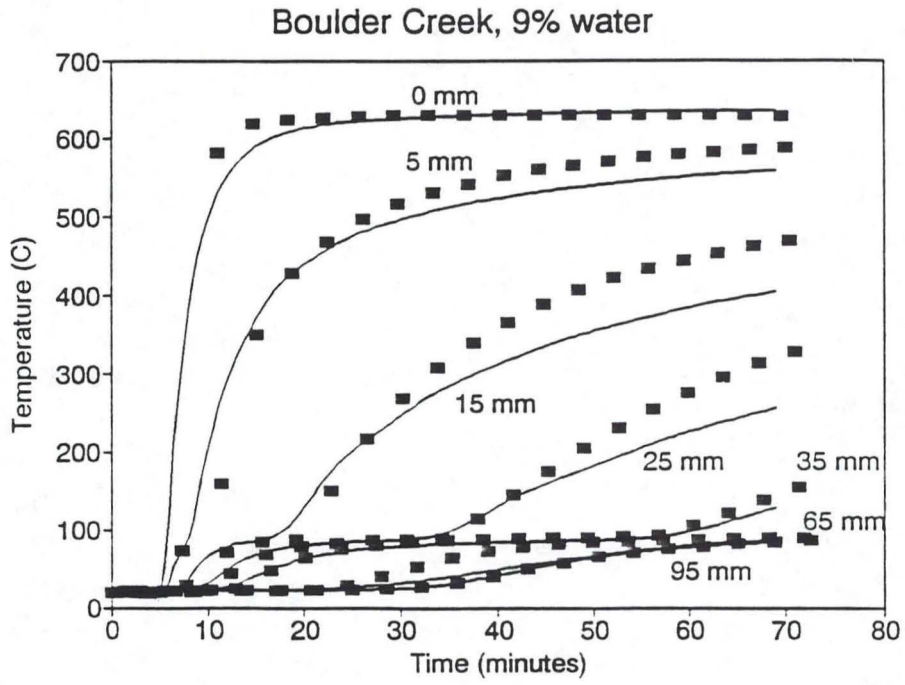
Boulder Creek, 9% water
Temperature (C)
Time (minutes)
0 mm
5 mm
15 mm
25 mm
35 mm
65 mm
95 mm

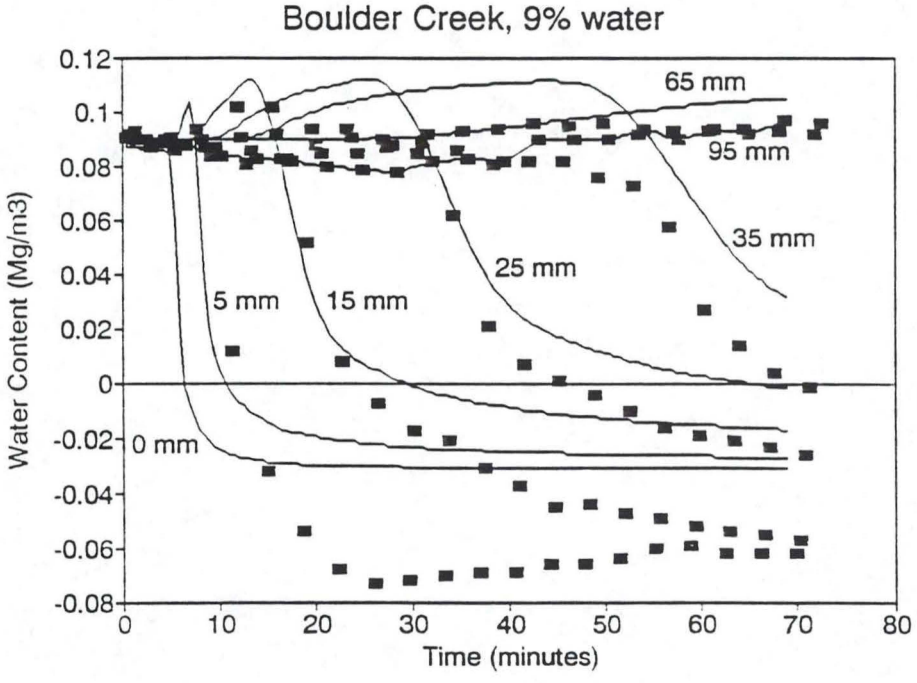
Boulder Creek, 9% water
Water Content (Mg/m3)
Time (minutes)
65 mm
95 mm
35 mm
25 mm
15 mm
5 mm
0 mm

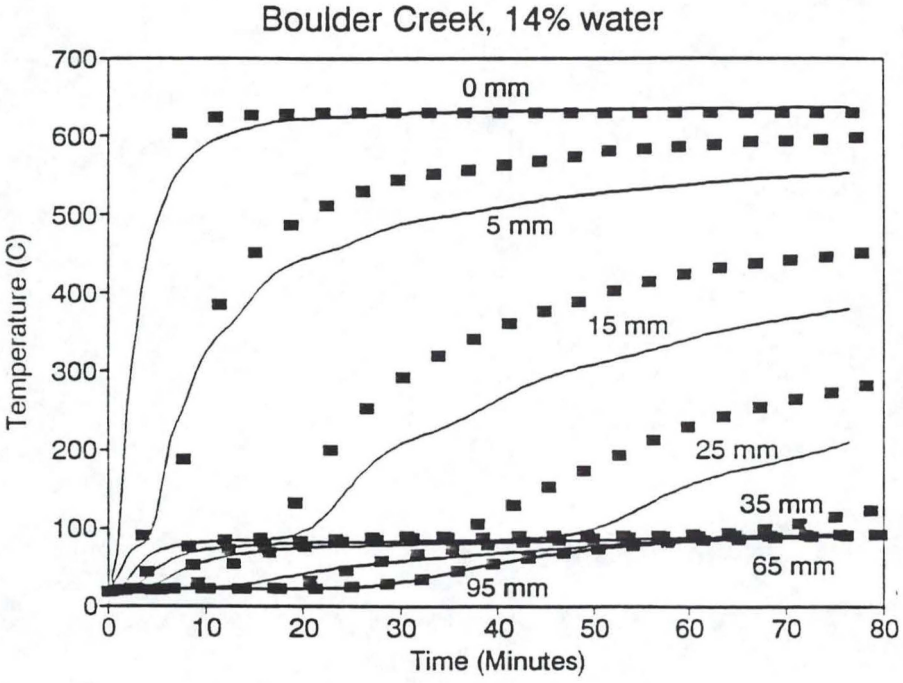
Boulder Creek, 14% water
Temperature (C)
Time (Minutes)
0 mm
5 mm
15 mm
25 mm
35 mm
65 mm
95 mm
700
600
500
400
300
200
100
0
0
10
20
30
40
50
60
70
80

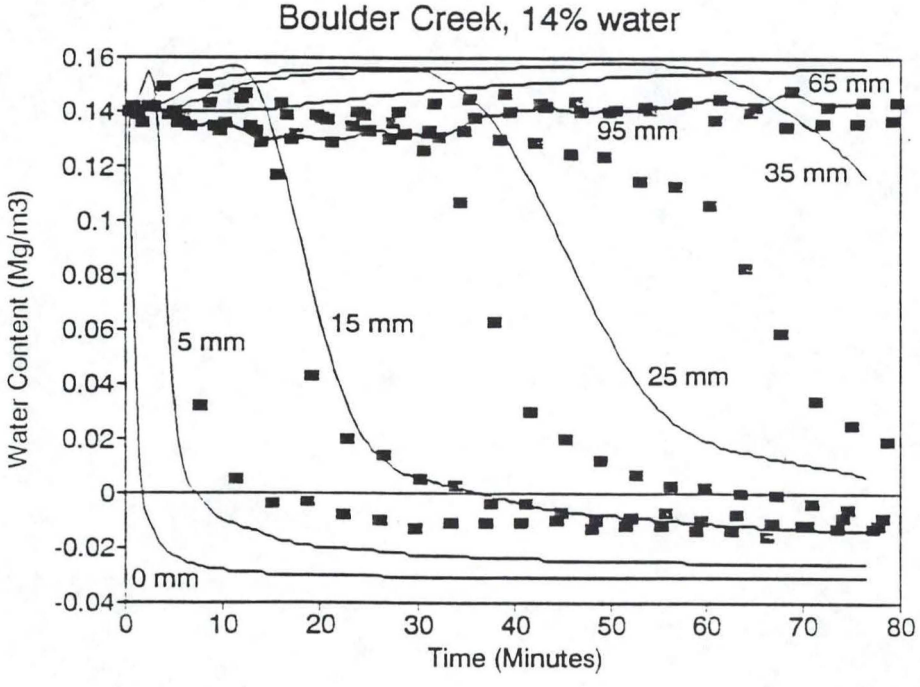
Boulder Creek, 14% water
Water Content (Mg/m3)
Time (Minutes)
65 mm
95 mm
35 mm
15 mm
5 mm
25 mm
0 mm
0.16
0.14
0.12
0.1
0.08
0.06
0.04
0.02
0
-0.02
-0.04
0
10
20
30
40
50
60
70
80

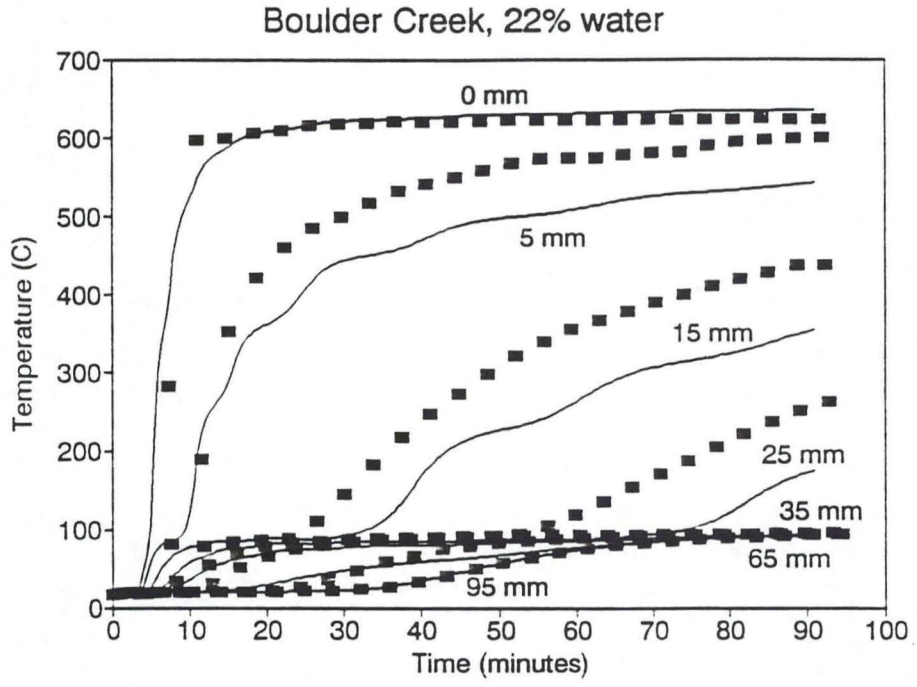
Boulder Creek, 22% water
Temperature (C)
Time (minutes)
0 mm
5 mm
15 mm
25 mm
35 mm
65 mm
95 mm
0
100
200
300
400
500
600
700
0
10
20
30
40
50
60
70
80
90
100

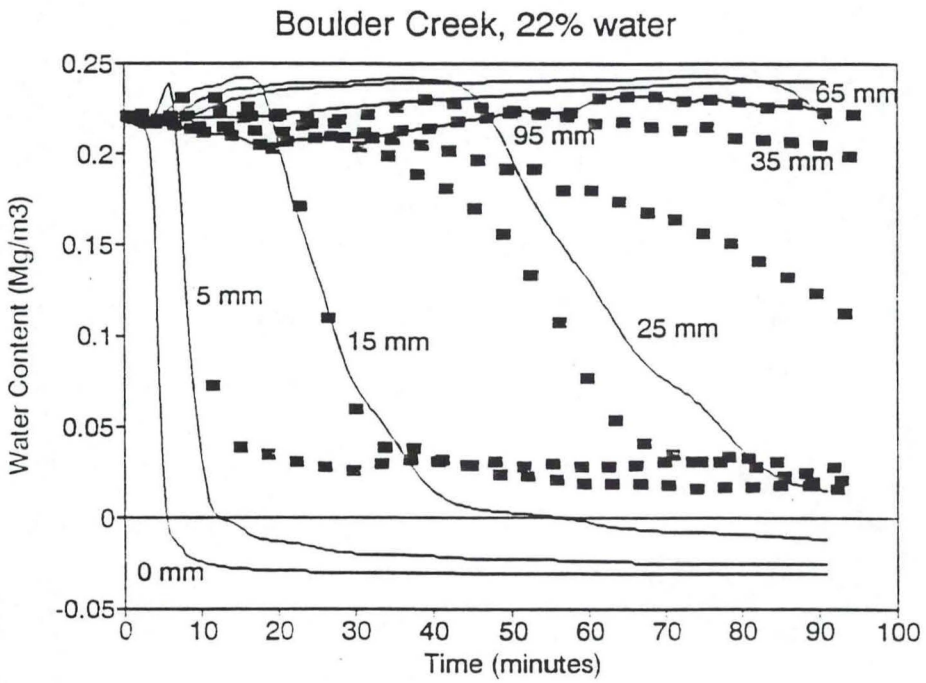
Boulder Creek, 22% water
Water Content (Mg/m3)
Time (minutes)
65 mm
95 mm
35 mm
5 mm
15 mm
25 mm
0 mm
-0.05
0
0.05
0.1
0.15
0.2
0.25
0
10
20
30
40
50
60
70
80
90
100

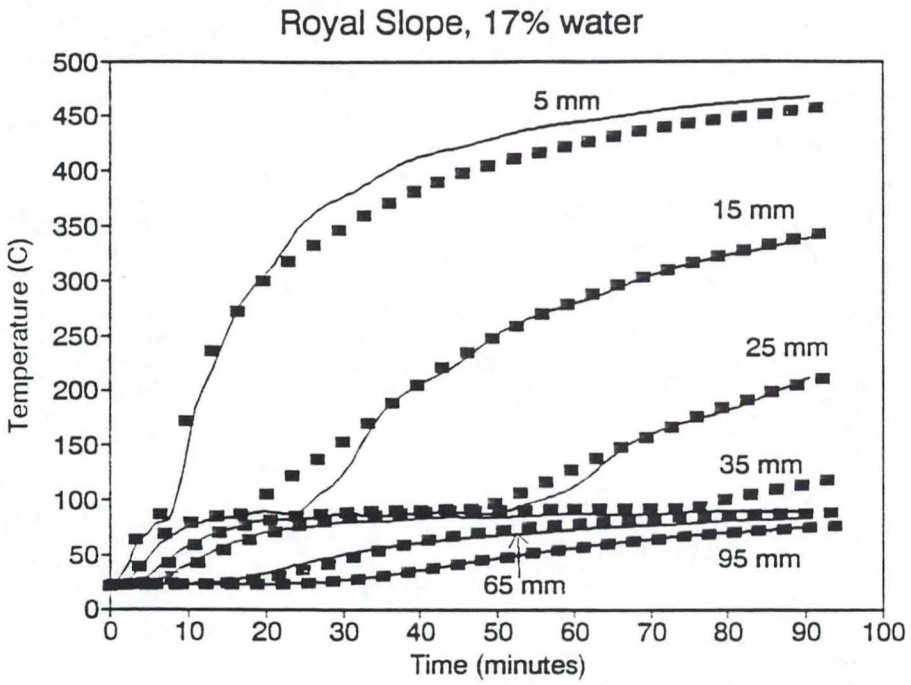
Royal Slope, 17% water
Temperature (C)
Time (minutes)
5 mm
15 mm
25 mm
35 mm
65 mm
95 mm
0
50
100
150
200
250
300
350
400
450
500
0
10
20
30
40
50
60
70
80
90
100

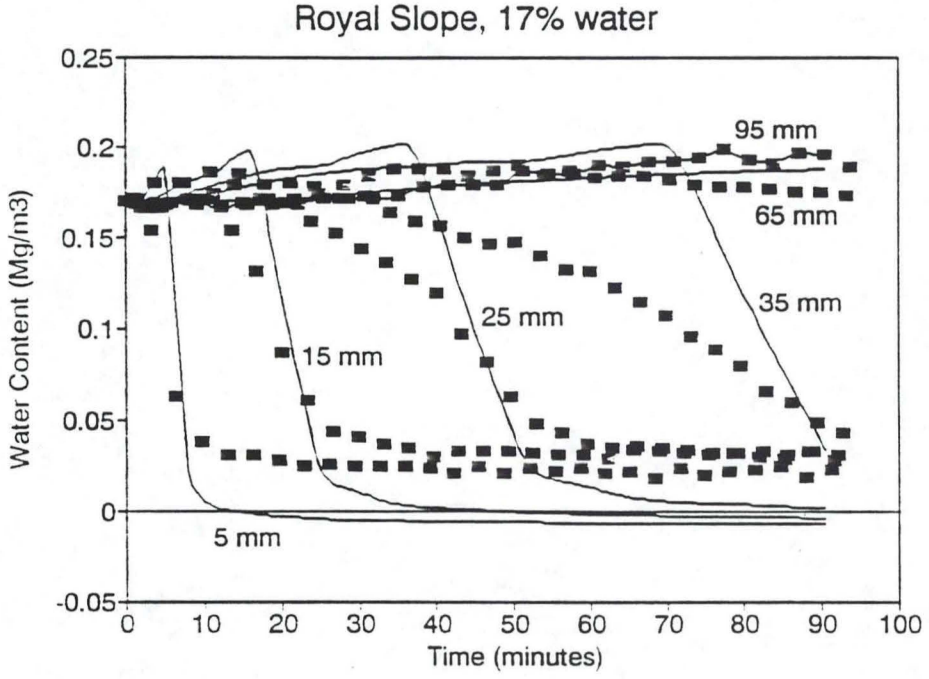
Royal Slope, 17% water
Water Content (Mg/m3)
Time (minutes)
95 mm
65 mm
35 mm
25 mm
15 mm
5 mm
-0.05
0
0.05
0.1
0.15
0.2
0.25
0
10
20
30
40
50
60
70
80
90
100

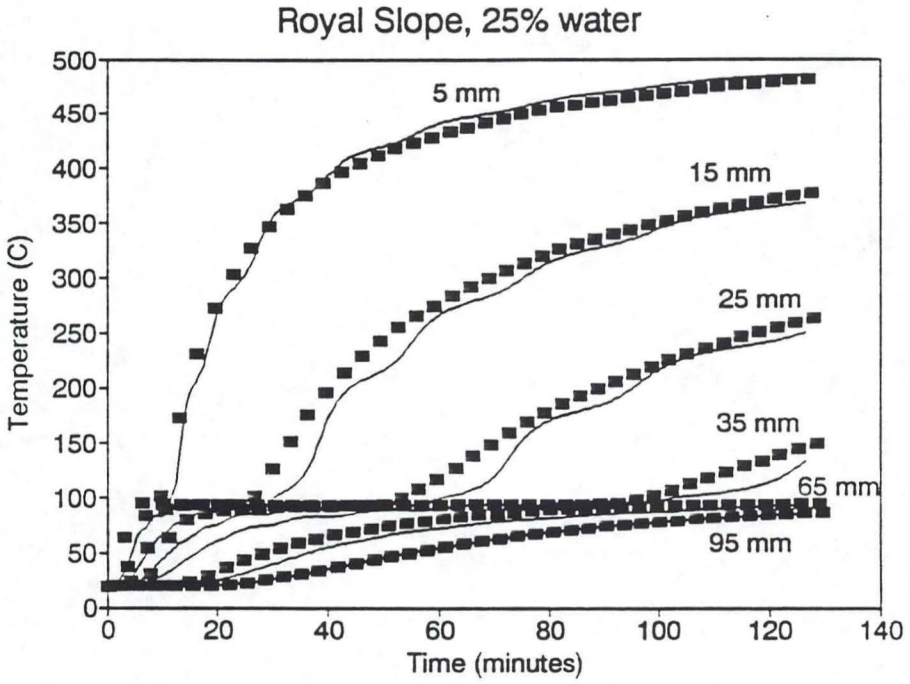
Royal Slope, 25% water
Temperature (C)
Time (minutes)
5 mm
15 mm
25 mm
35 mm
65 mm
95 mm
0
50
100
150
200
250
300
350
400
450
500
0
20
40
60
80
100
120
140

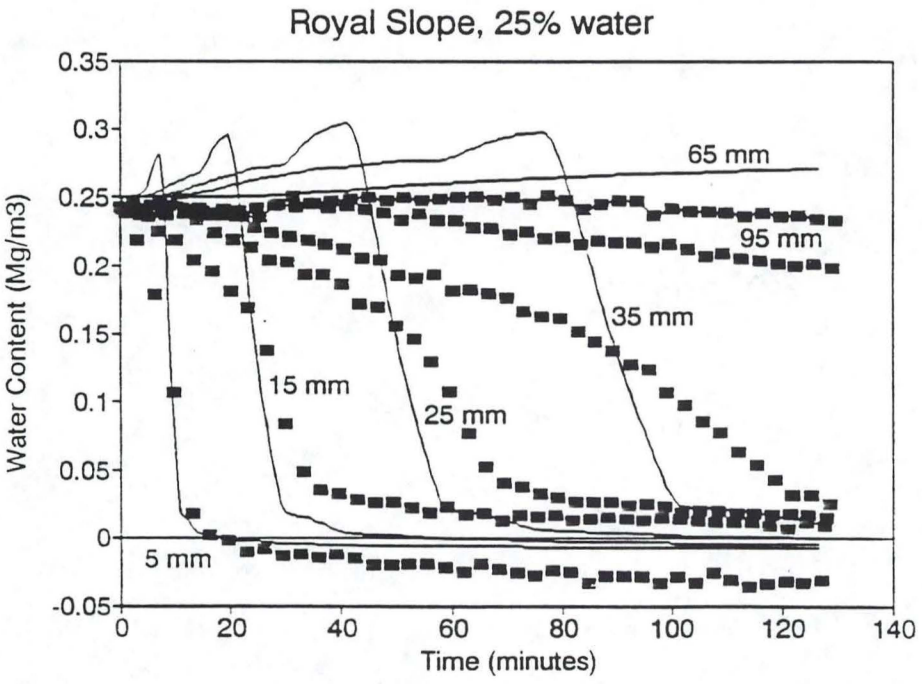
Royal Slope, 25% water
Water Content (Mg/m3)
Time (minutes)
65 mm
95 mm
35 mm
15 mm
25 mm
5 mm
-0.05
0
0.05
0.1
0.15
0.2
0.25
0.3
0.35
0
20
40
60
80
100
120
140

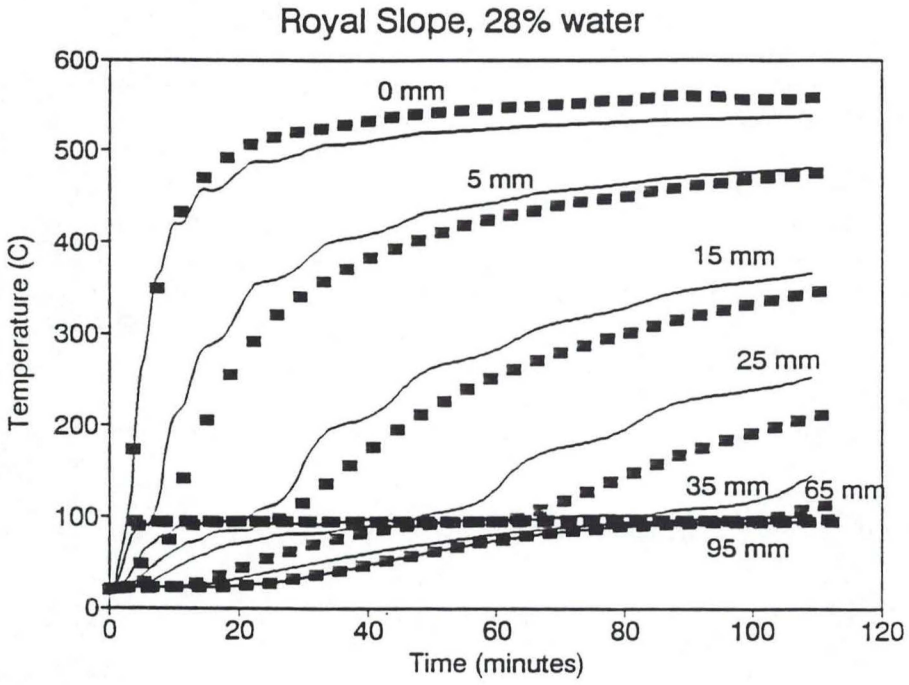
Royal Slope, 28% water
Temperature (C)
Time (minutes)
0 mm
5 mm
15 mm
25 mm
35 mm
65 mm
95 mm
600
500
400
300
200
100
0
0
20
40
60
80
100
120

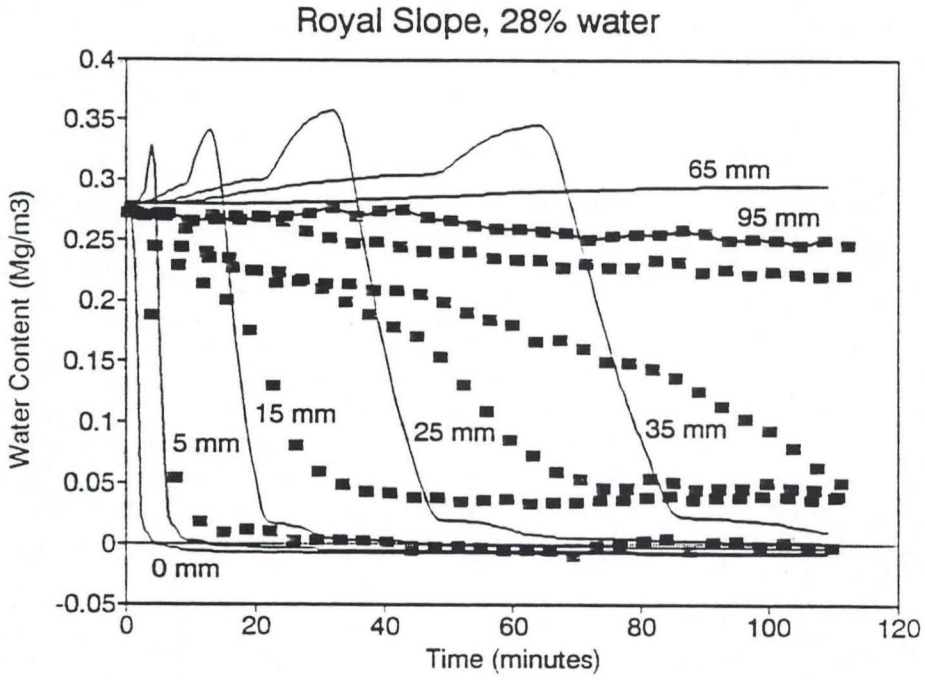
Royal Slope, 28% water
Water Content (Mg/m3)
Time (minutes)
65 mm
95 mm
15 mm
5 mm
25 mm
35 mm
0 mm
0.4
0.35
0.3
0.25
0.2
0.15
0.1
0.05
0
-0.05
0
20
40
60
80
100
120

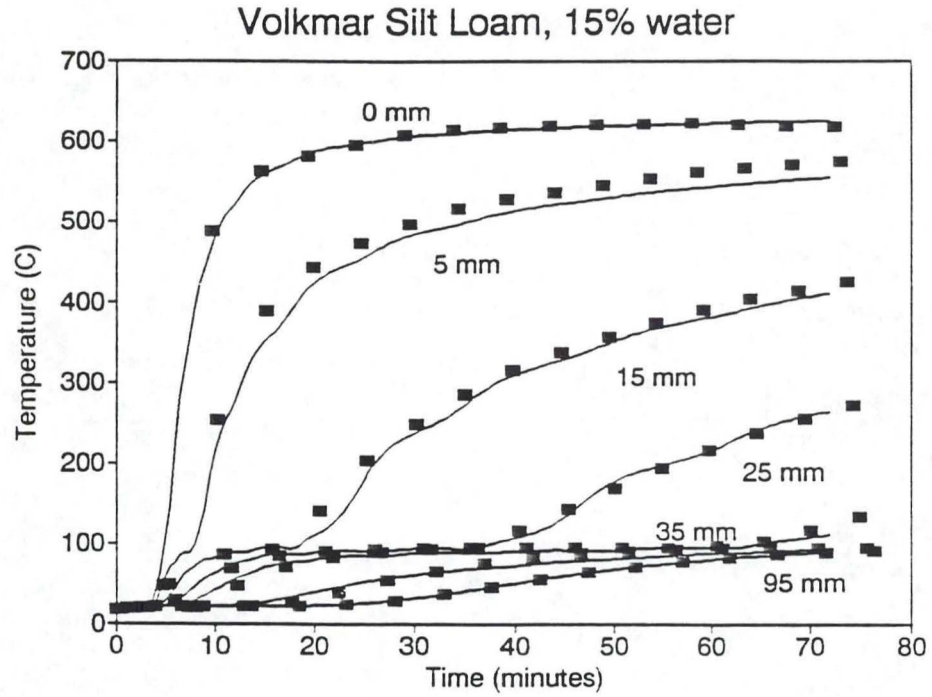
Volkmar Silt Loam, 15% water
Temperature (C)
Time (minutes)
0 mm
5 mm
15 mm
25 mm
35 mm
95 mm
0
100
200
300
400
500
600
700
0
10
20
30
40
50
60
70
80

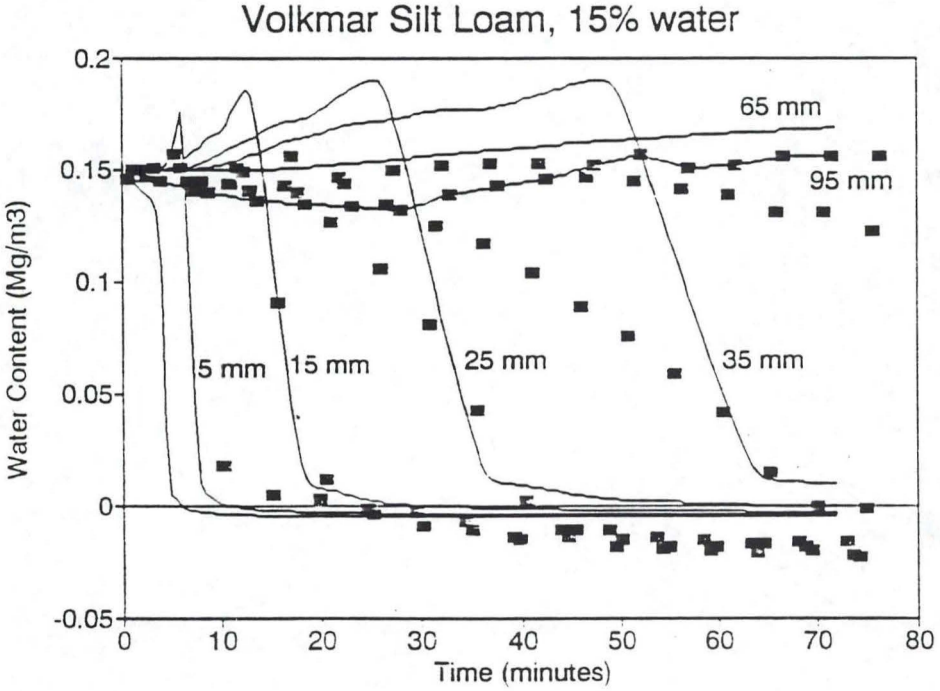
Volkmar Silt Loam, 15% water
Water Content (Mg/m3)
Time (minutes)
65 mm
95 mm
5 mm
15 mm
25 mm
35 mm
-0.05
0
0.05
0.1
0.15
0.2
0
10
20
30
40
50
60
70
80

Fig 14

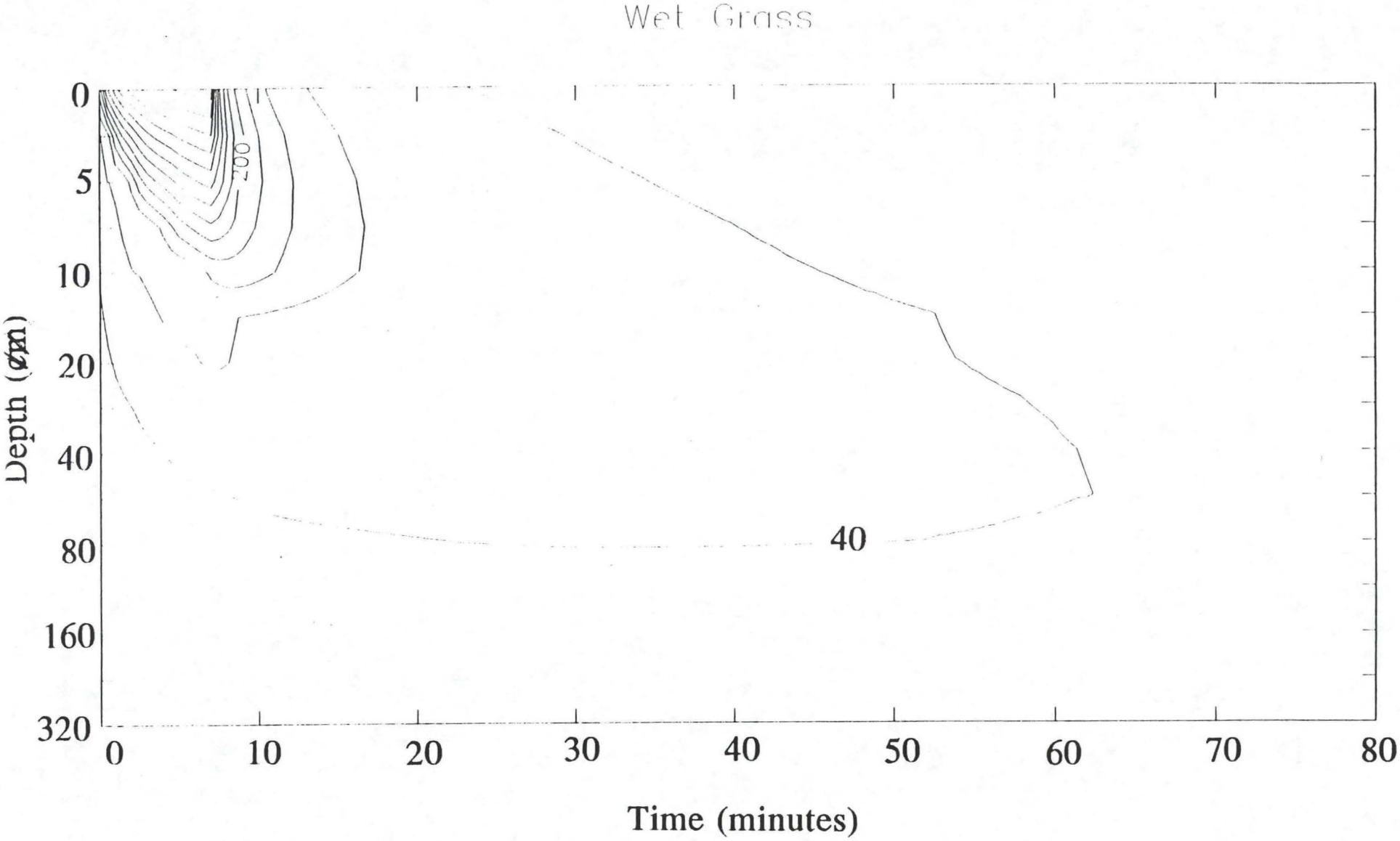
Wet Grass
0
5
10
20
40
80
160
320
Depth (cm)
.002
40
0
10
20
30
40
50
60
70
80
Time (minutes)

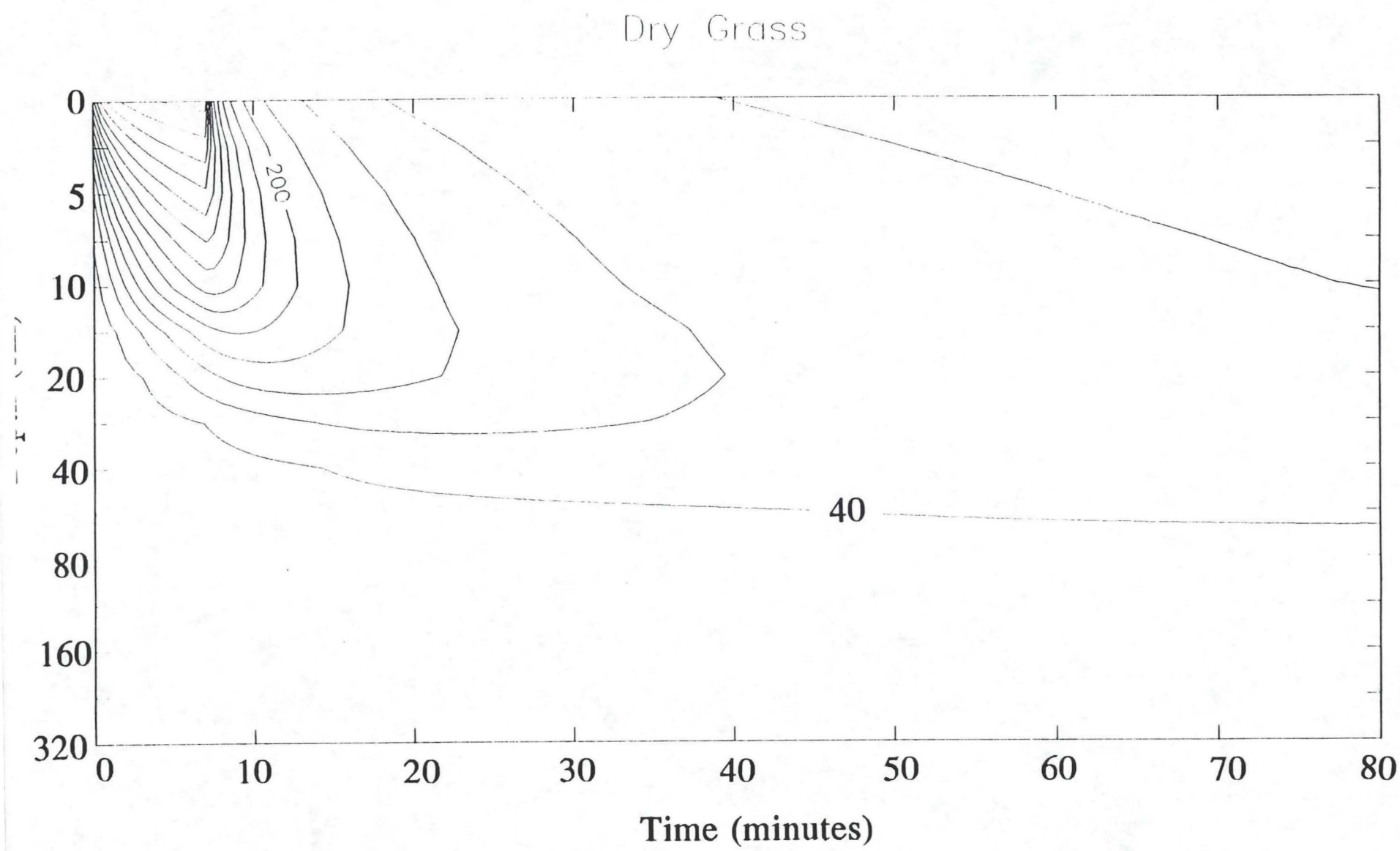
Dry Grass
0
5
10
20
40
80
160
320
200
40
0
10
20
30
40
50
60
70
80
Time (minutes)

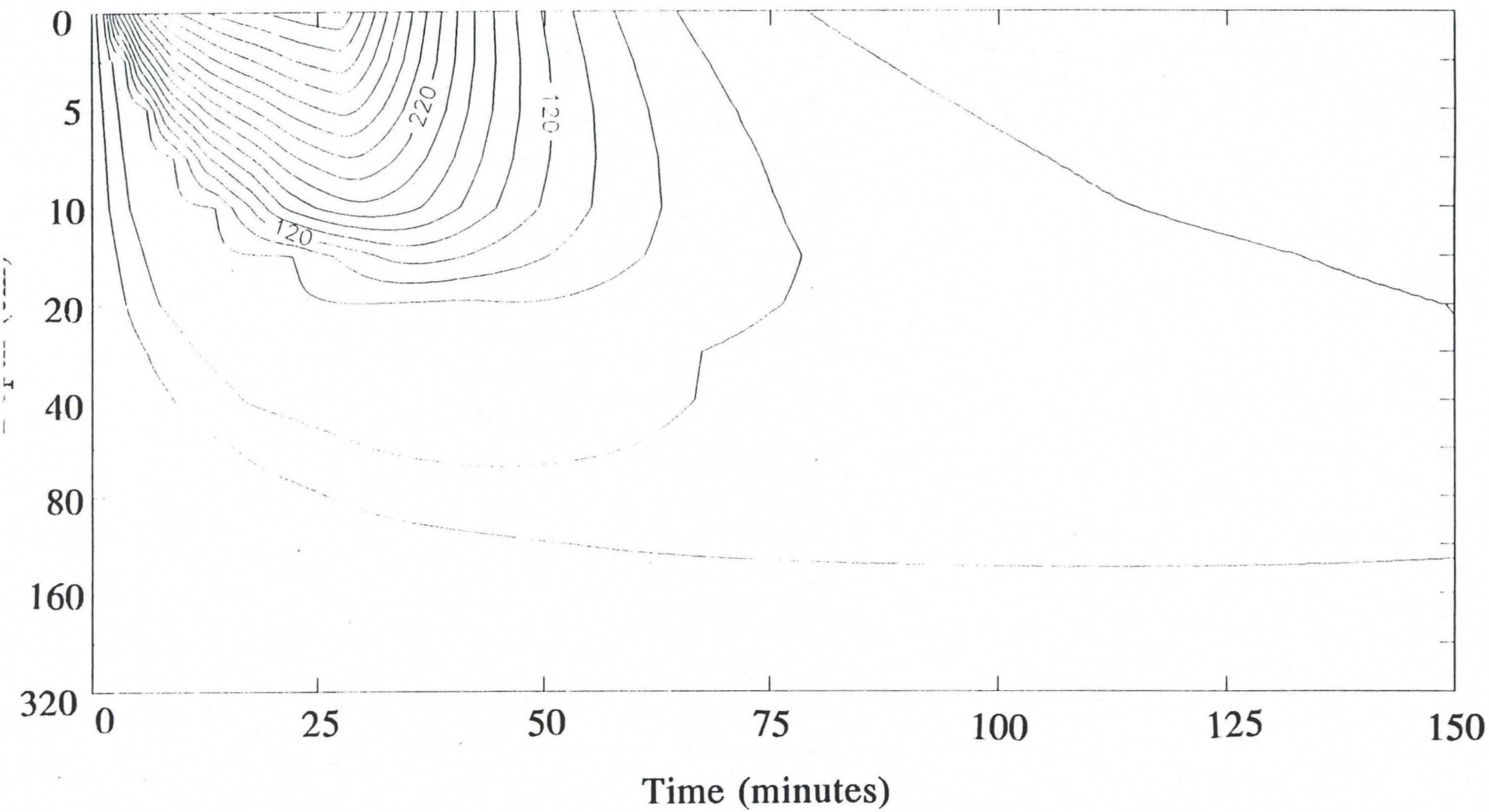
Wet Shrub
0
5
10
20
40
80
160
320
220
120
120
0
25
50
75
100
125
150
Time (minutes)

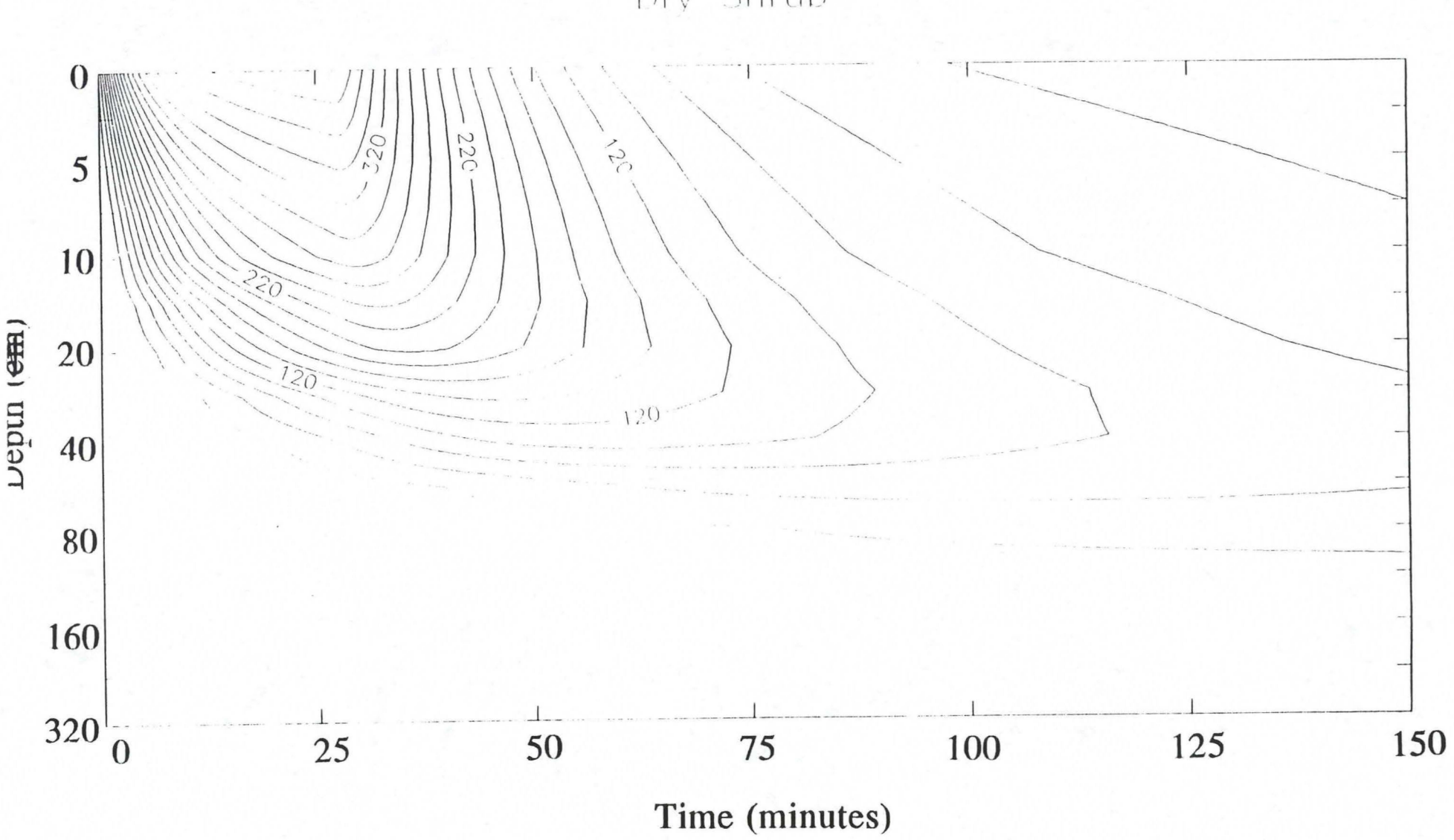
Dry Shrub
0
5
10
20
40
80
160
320
320
220
120
220
120
120
0
25
50
75
100
125
150
Time (minutes)

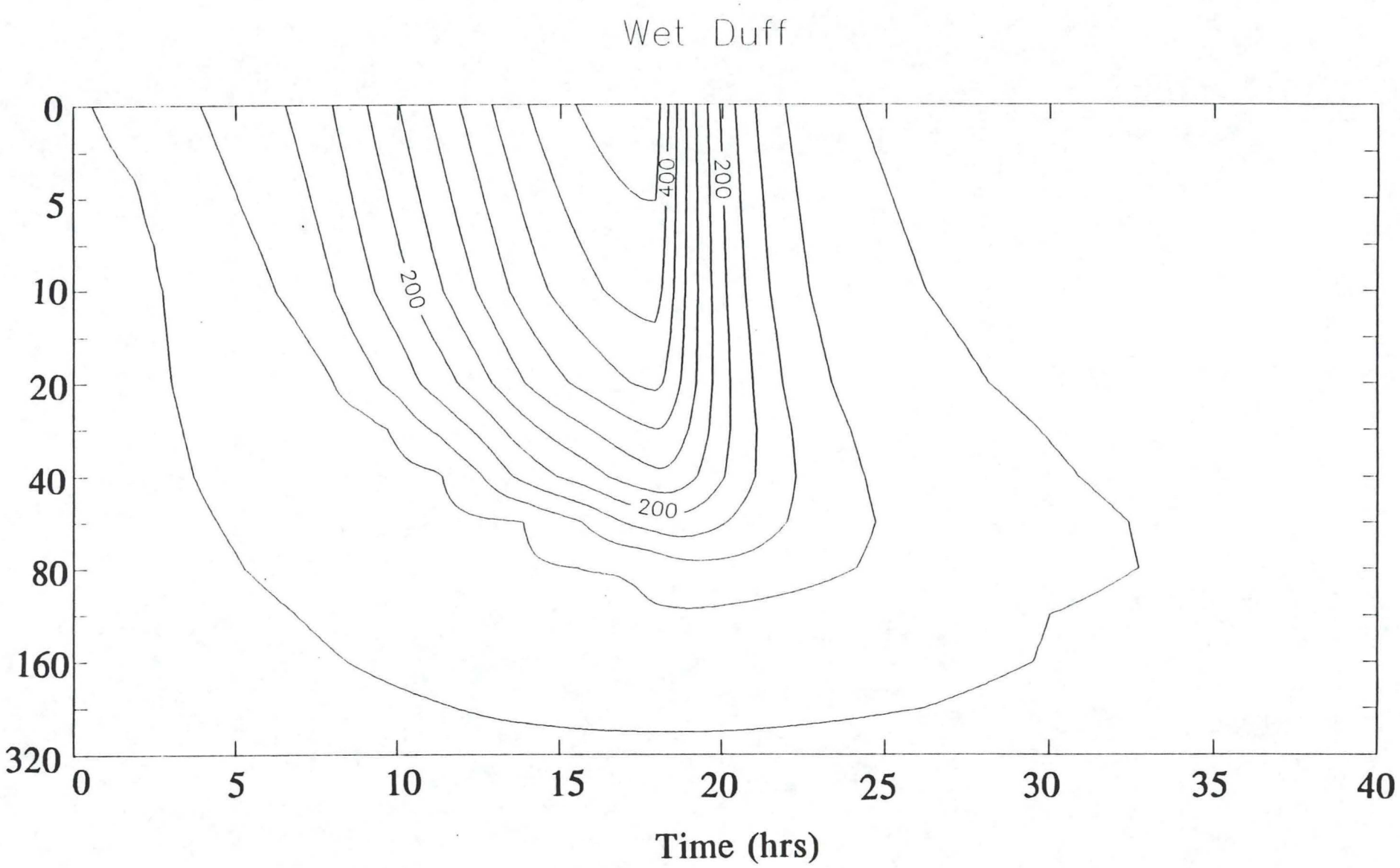
Wet Duff
0
5
10
20
40
80
160
320
0
5
10
15
20
25
30
35
40
Time (hrs)
400
200
200
200

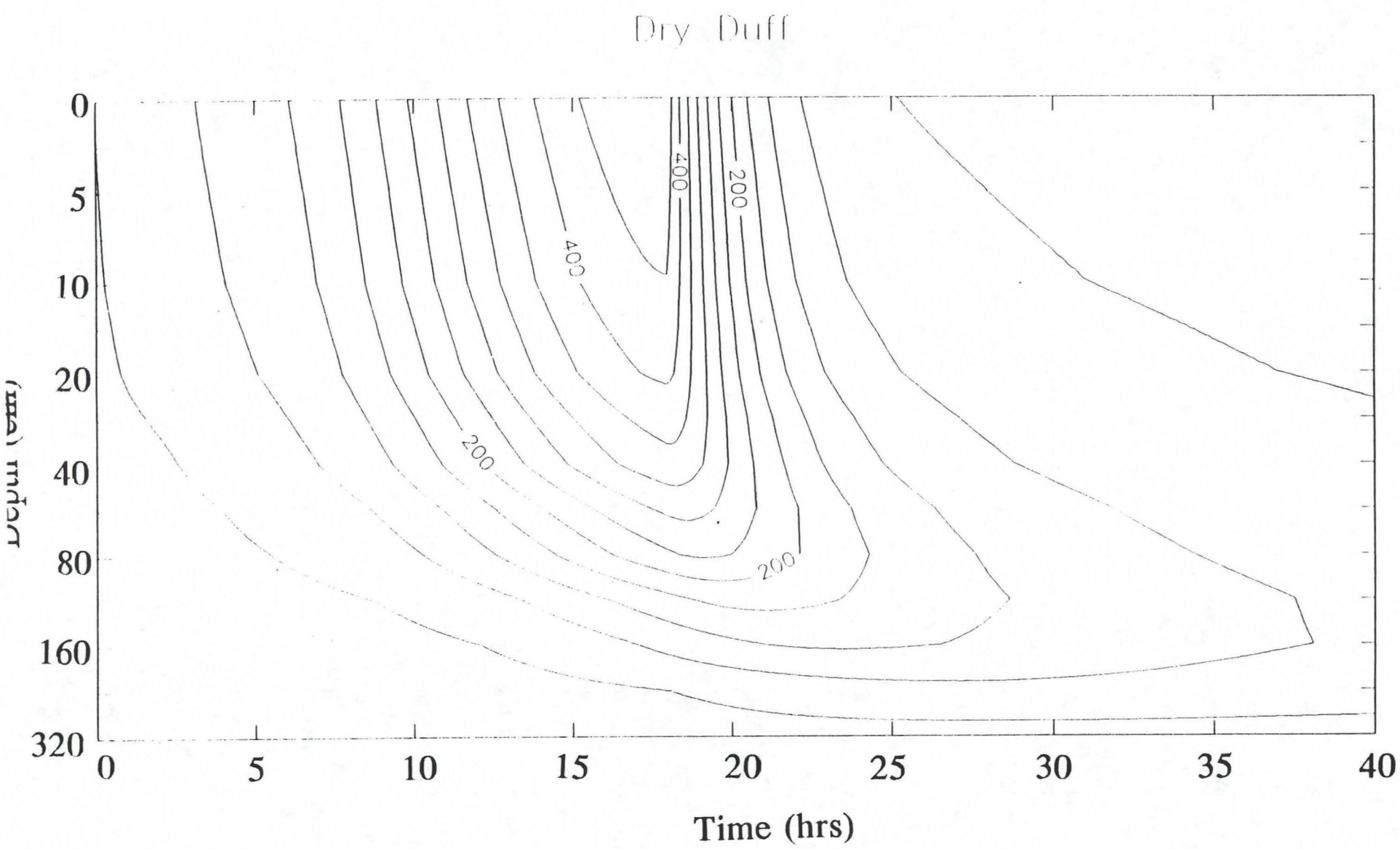
Dry Duff
0
5
10
20
40
80
160
320
Depth (mm)
400
400
200
200
200
0
5
10
15
20
25
30
35
40
Time (hrs)

Appendix A. Program to determine temperature of soil that is heated to high temperatures at the surface.

```
uses math, scrplt2, graph, crt;
{$R+}
const mmax = 15;      {maximum number of simulation nodes }
      Patm = 92000; {atmospheric pressure at Pullman, Pa}
      Dvo = 2.12e-5;
      Tstd = 273.15;
      Po = 101300;
      R = 8.3143 ;
      Mw = 0.018;

type real = double;
     rsubs = 0..mmax;
     rvectors = array[rsubs] of real;    {Temps. and water contents}
     datavecs = array[0..50] of real;    {input data for boundary cond.}
     plotvecs = array[rsubs] of byte;    {depths to plot}

function humidity(p,t:real; var dhdp:real):real;
  var h,Tk:real;
  begin
    Tk:=t+Tstd;
    h:=exp(Mw*p/(R*Tk));
    dhdp:=Mw*h/(R*Tk);
    humidity:=h;
  end;

function watercontent(p, xo:real; var dwdp:real):real;
  const lnpo = 13.82;  {ln of oven dry water content}
  begin
    if p>=0 then p:=-0.001;
    dwdp:=-xo/(lnpo*p);
    watercontent:=xo*(1-ln(-p)/lnpo);
  end;

function vaporpressure(t:real):real;    {returns vapor pressure in Pa}
  begin
    t:=1-373.15/(t+273.15);
    vaporpressure:=101325*exp(t*(13.3016+t*(-2.042+t*(0.26+t*2.69))));
  end;

function slope(t,p:real):real;       {returns slope of vp curve; Pa/C}
  var dydt,Tk:real;
  begin                                  {t in deg. C, p in pascals}
    Tk:=t+Tstd;
    t:=1-373.15/Tk; dydt:=373.15/sqr(Tk);
    slope:=p*dydt*(13.3015+t*(-4.082+t*(0.78+t*10.76)));
  end;

function Hv(t:real):real; {returns latent heat of vaporization in J/kg}
  begin                        {t in deg. C}
    Hv:=2.508e6-2670*t;
```

```
  end;

function Kvap(t,p:real):real;  {returns vapor conductivity in kg/(m s Pa)}
  var Tk,Dv,stcor:real;
  begin
    Tk:=t+Tstd;;
    Dv:=Dvo*(Po/Patm)*pow(Tk/Tstd,1.75);
    stcor:=1-p/Patm;
    if stcor<0.3 then stcor:=0.3;
    Kvap:=Mw*Dv/(R*Tk*stcor);
  end;

function tcond(t,xw,xs,ls,ga,xwo,cop,p,s:real; var enh:real):real;
  {t in deg. C, xw,xs:vol fract water, solid; p is actual vapor
   pressure (Pa); s is slope (Pa/C)}
  var wf,ka,ks,kw,la,lw,lf,xa,xws,gc,lda,xv,tc:real;
    begin       {xw is vol wc}
      xws:=1-xs; xa:=xws-xw;
      if t<100 then begin
        lw:=0.554+t*(2.24e-3-9.87e-6*t);
        tc:=sqr(sqr((t+273)/303));
      end
      else begin
        lw:=0.68; tc:=2.3;
      end;
      lda:=0.024+t*(7.73e-5-2.6e-8*t);
      if xw<0.01*xwo then wf:=0
      else wf:=1/(1+pow(xw/xwo,-cop*tc));
      la:=lda+wf*Hv(t)*s*Kvap(t,p);
      gc:=1-2*ga; lf:=la+(lw-la)*wf;
      ka:=(2/(1+(la/lf-1)*ga)+1/(1+(la/lf-1)*gc))/3;
      kw:=(2/(1+(lw/lf-1)*ga)+1/(1+(lw/lf-1)*gc))/3;
      ks:=(2/(1+(ls/lf-1)*ga)+1/(1+(ls/lf-1)*gc))/3;
      enh:=(1+2*wf)*ka;
      tc:=(kw*lw*xw+ka*la*xa+ks*ls*xs)/(kw*xw+ka*xa+ks*xs);
      if (tc>0) and (tc<5) then tcond:=tc else tcond:=1;
  end;

procedure readdata(var mplus1,ptmax:integer;
                   var hc,heaton,startvp,heatvp,HeaterRabs,Tair,
                   TimeConst,bd,pd,xo,ls,ga,xwo,cop,starttemp,startwc:real;
                   var z:rvectors;
                   var plotnode:plotvecs;
                   var t,bt,bw:datavecs);
  var q,i,psum:integer;
      ti,newti,ts,ws:real;          {Reads data from a data file, initiates}
      infile:text;                  {graphics, and plots the data.  Returns}
      filename:string[20];          {average starting temperature and water}
  begin                               {content of the soil column and the    }
    clrscr;  psum:=0;                 {lower boundary temperature             }
    write('datafile name '); readln(filename);
    assign(infile,filename); reset(infile);
    readln(infile,mplus1);
```

```
    for i:=0 to mplus1 do begin
      readln(infile,z[i],plotnode[i]); z[i]:=z[i]/1000;
      if plotnode[i]=1 then psum:=psum+1;
    end;
    readln(infile,hc);
    readln(infile,heaton);
    readln(infile,startvp);
    readln(infile,heatvp);
    readln(infile,HeaterRabs);
    readln(infile,Tair);
    readln(infile,TimeConst);
    readln(infile,bd);
    readln(infile,pd);
    readln(infile,xo);
    readln(infile,ls);
    readln(infile,ga);
    readln(infile,xwo);
    readln(infile,cop);
    readln(infile,startwc);
    graphsetup(0.2,0.8,0.05,0.4,1);
    scale(0,6000,0,700,1);
    axes(0,0,1000,100,true,1);
    graphsetup(0.2,0.8,0.5,0.9,2);
    scale(0,6000,-0.05,0.5,2);
    axes(0,0,1000,0.05,true,2);
    setbkcolor(1);setcolor(15); directvideo:=false;
    ti:=0; q:=1; i:=1; starttemp:=0;
    while not eof(infile) do begin
      readln(infile,newti,ts,ws);
      if newti<ti then q:=q+1;
      ti:=newti;
      pointplt(ti,ts,1,1);
      pointplt(ti,ws,1,2);
      if q=psum then begin                    {save the bottom temperatures}
        t[i]:=ti; bt[i]:=ts; bw[i]:=ws; i:=i+1;
      end;
    end;
    close(infile);
    starttemp:=bt[1]; ptmax:=i-2;
    t[0]:=0; bt[0]:=bt[1]; bw[0]:=bw[1];
  end;

const PlotFile:boolean = false;

var conv,vcon,p,z,kv,psat,h,w,wn,t,tn,v,kh,ke,
    kev,cp,s,AirPor,Hvap,dwdp,dhdp,u,enh:rvectors;
    ptr,ptrmax,i,m,mplus1:integer;
    starttemp,startwc,epse,epsw,xw,dt,ti,xws,xs,ch,cop,TimeConst:real;
    gvol,dC,dv,dCdt,dCdp,dvdp,dvdt,seh,sev,dtn,dJv,dJvdt,dJvdp,cenh:real;
    ls,ga,xwo,exf,Rabs,bd,pd,Tor,dw,hc,t0,t1,w0,w1,ft,tmax,wav:real;
    ms,ns,xo,heaton,heatvp,Tair,HeaterRabs,startvp,tk,tk3,airvp:real;
    tim,Tlb,wlb:datavecs;
    plotnode:plotvecs;
```

```
    outfile:text; filename:string[30];
begin
{Simulation Parameters                                                    }
  dt:=30;                    {time step - s                               }
  epse:=100;                 {energy balance error - W/m2                  }
  epsw:=1e-5;                {water mass balance error - kg/(m2 s)       }
  dw:=1000;                   {density of water - kg/m3                   }
  tor:=0.66;                 {soil tortuosity - dimensionless            }
if plotfile then begin
  write('file name for plot file '); readln(filename);
  assign(outfile,filename);
  rewrite(outfile);
end;
{Initialization                                                           }
  readdata(mplus1,ptrmax,hc,heaton,startvp,heatvp,HeaterRabs,Tair,TimeConst,
           bd,pd,xo,ls,ga,xwo,cop,starttemp,startwc,z,plotnode,tim,Tlb,wlb);
  m:=mplus1-1; ti:=0; ptr:=1;
  xs:=bd/pd; xws:=1-xs; cenh:=1+2.6/sqrt(1.3*xo-0.034);
  for i:=1 to m do v[i]:=0.5*(z[i+1]-z[i-1]);
  for i:=0 to mplus1 do begin
    t[i]:=starttemp; tn[i]:=starttemp; w[i]:=startwc;
    p[i]:=-exp(13.82*(1-w[i]/xo));
    w[i]:=watercontent(p[i],xo,dwdp[i]);
    h[i]:=humidity(p[i],t[i],dhdp[i]);
    wn[i]:=w[i];
    Kev[i]:=0; u[i]:=0; enh[i]:=0;
  end;
  tmax:=tim[ptrmax]; t0:=tlb[0]; t1:=tlb[1]; w0:=wlb[0]; w1:=wlb[1];
  AirPor[0]:=1;
{Begin Simulation                                                         }
  while ti<tmax do begin
    ti:=ti+dt;
    if ti>tim[ptr] then begin      {set lower boundary conditions}
      ptr:=ptr+1;
      t0:=t1; t1:=tlb[ptr]; w0:=w1; w1:=wlb[ptr];
    end;
    ft:=(ti-tim[ptr-1])/(tim[ptr]-tim[ptr-1]);  {use linear interpolation}
    tn[mplus1]:=t0+ft*(t1-t0);
    wn[mplus1]:=w0+ft*(w1-w0);
    p[mplus1]:=-exp(13.82*(1-wn[mplus1]/xo));
    h[mplus1]:=humidity(p[mplus1],t[mplus1],dhdp[mplus1]);
    if ti<heaton then begin          {set the surface boundary conditions}
      tn[0]:=starttemp; Rabs:=0; airvp:=startvp;
    end
    else begin
      exf:=(1-exp(-(ti-heaton)/TimeConst));
      tn[0]:=Tair*exf;
      Rabs:=HeaterRabs*exf;
      airvp:=heatvp*exf;
    end;
    repeat                         {begin heat and water solutions}
      seh:=0; sev:=0;
      ke[0]:=hc;
```

```
  kev[0]:=6.2e-9*hc; {6.2e-9*hc makes heat and water cond. equal}
  psat[0]:=vaporpressure(tn[0]); h[0]:=airvp/psat[0];
  psat[1]:=vaporpressure(tn[1]); wav:=0.5*(wn[1]+wn[2]);
  s[1]:=slope(tn[1],psat[1]); Hvap[1]:=Hv(tn[1]);
  kh[1]:=tcond(tn[1],wav,xs,ls,ga,xwo,cop,h[1]*psat[1],s[1],enh[1]);
  AirPor[1]:=(xws-wav);
  kv[1]:=enh[1]*AirPor[1]*tor*Kvap(t[1],psat[1]*h[1]);
  for i:=1 to m do begin
    cp[i]:=v[i]*(0.87*bd+4.18e6*wn[i])/dt;
    psat[i+1]:=vaporpressure(tn[i+1]);
    if i<m then wav:=0.5*(wn[i+1]+wn[i+2]) else wav:=wn[mplus1];
    conv[i]:=0.5*(u[i-1]+u[i])*1200*293/(0.5*(tn[i+1]+tn[i+2])+273);
    vcon[i]:=conv[i]*Mw/(R*1200*293);
    s[i+1]:=slope(tn[i+1],psat[i+1]); Hvap[i+1]:=Hv(tn[i+1]);
    kh[i+1]:=tcond(tn[i+1],wav,xs,ls,ga,xwo,cop,
                   h[i+1]*psat[i+1],s[i+1],enh[i+1]);
    ke[i]:=(kh[i])/((z[i+1]-z[i]))+conv[i];
    AirPor[i+1]:=(xws-wav);
    kv[i+1]:=enh[i+1]*AirPor[i+1]*tor*Kvap(t[i+1],psat[i+1]*h[i+1]);
    kev[i]:=(kv[i]+kv[i+1])/(2*(z[i+1]-z[i]))+vcon[i];
    dJv:=kev[i-1]*(psat[i]*h[i]-psat[i-1]*h[i-1])
        -kev[i]*(psat[i+1]*h[i+1]-psat[i]*h[i]);
    dJvdt:=s[i]*h[i]*(kev[i-1]+kev[i]);
    dJvdp:=psat[i]*(kev[i-1]+kev[i])*dhdp[i];
    dC:=ke[i-1]*(tn[i]-tn[i-1])-ke[i]*(tn[i+1]-tn[i])
        +cp[i]*(tn[i]-t[i])-Hvap[i]*dw*v[i]*(wn[i]-w[i])/dt;
    dv:=dJv+dw*v[i]*(wn[i]-w[i])/dt;
    dCdp:=-Hvap[i]*dw*v[i]*dwdp[i]/dt;
    dvdp:=dJvdp+dw*v[i]*dwdp[i]/dt;
    dvdt:=dJvdt;
    dCdt:=ke[i]+ke[i-1]+cp[i];
    if (i=1) then begin
      tk:=tn[1]+273; tk3:=tk*tk*tk;
      dC:=dC-Rabs+0.9*5.67e-8*tk*tk3;
      dCdt:=dCdt+4*0.9*5.67e-8*tk3;
    end;
    sev:=sev+abs(dv);
    seh:=seh+abs(dC);
    dtn:=(dv*dCdp-dC*dvdp)/(dCdp*dvdt-dCdt*dvdp);
    if dtn<-100 then dtn:=-100;
    tn[i]:=tn[i]-dtn;
    dtn:=(dv-dvdt*dtn)/dvdp; p[i]:=p[i]-dtn;
    if p[i]>0 then p[i]:=(p[i]+dtn)*0.5;
    if p[i]<-1e20 then p[i]:=-1e20;
    wn[i]:=watercontent(p[i],xo,dwdp[i]);
    h[i]:=humidity(p[i],tn[i],dhdp[i]);
  end;
  gotoxy(10,1); write(sev:8,' ',seh:8);
until (sev < epsw) and (seh < epse);
u[m]:=0;
for i:=m downto 1 do begin          {calculate conv. air velocity}
  gvol:=dw*v[i]*R*(tn[i]+273)*(w[i]-wn[i])/(dt*AirPor[i]*Mw*Patm);
  if gvol<0 then gvol:=0;
```

```
      u[i-1]:=u[i]+gvol;
    end;
    for i:=1 to mplus1 do begin
      ch:=wn[i]-w[i]; w[i]:=wn[i]; wn[i]:=w[i]+ch;
      ch:=tn[i]-t[i]; t[i]:=tn[i]; tn[i]:=t[i]+ch;
      if plotnode[i]>0 then begin
        pointplt(ti,w[i],0,2); pointplt(ti,t[i],0,1);
      end;
    end;
    if plotfile then begin
      write(outfile,ti:5:0);
      for i:=1 to mplus1 do begin
        if plotnode[i]>0 then write(outfile,t[i]:6:1,w[i]:7:3);
      end;
      writeln(outfile);
    end;
  end;
  ptr:=0; readln(ptr); if ptr<>0 then hpscreendump;
  close(outfile);
end.
```

Appendix B. Example input file for the model giving model parameters and measured values. Measured values show only the first and start of the second depths.

```
14                  {number of solution nodes plus 1}
0    0              {depths of the solution nodes in mm}
0    1              {a 1 in the second column means plot the }
2.5  0
5    1              {simulated value for that node}
7.5  0
10   0              {also means that there are measured data for that node}
15   1
20   0
25   1
30   0
35   1
40   0
50   0
65   1
95   1
20              {boundary layer conductance - W/(m2 C)          }
100             {delay from simulation start to heater on - s  }
1000            {starting vapor pressure of air - Pa           }
15000           {vapor pressure during heating - Pa             }
40000           {Rabs of heater when on - W/m2                    }
500             {air temperature during heating - C             }
200             {time constant for heater - s                   }
1.31e6          {soil bulk density - g/m3                       }
2.65e6          {soil particle density - g/m3                   }
0.37            {extrapolated water cont. at -1 J/kg, xw1       }
2.0             {thermal conductivity of mineral fraction      }
0.074           {de Vries shape factor                          }
0.23            {water content for liquid return flow, xwo     }
5.83            {cutoff power, qo                               }
0.07            {starting water content                        }
      1.4   22.882     0      {Time, Temperature, Water content data}
    220.4   252.13     0      {starting with surface                 }
    439.4   560.51     0
    659.4   605.34     0
    878.4   618.16     0
   1097.4   624.52     0
   1317.4    628.1     0
   1537.4    629.4     0
   1756.4   629.48     0
   1976.4   629.48     0
   2195.4   629.23     0
   2414.4   629.11     0
   2634.4   628.52     0
   2853.4    627.4     0
   3073.4   625.87     0
   3293.4    626.5     0
     26.3   22.927   0.072      {same data for next measurement depth}
    245.3   72.076   0.063
```

Predicting Thermal Conductivity of Soil at High Temperature

G. S. Campbell, J. Jungbauer, W. R. Bidlake and R. D. Hungerford

Introduction

When biomass on or above a soil surface burns, a heat pulse penetrates the soil. The resulting high soil temperatures can alter soil properties and kill roots and soil microbes. Since burning is often used as a management tool by foresters and range managers, it is important to know what soil and fuel conditions will be least detrimental to biological and physical properties. Since numerous factors affect the temperatures reached at different soil depths, and burn experiments are expensive and difficult to conduct, a modeling approach seems appropriate for prediction of soil temperatures under burns. One requirement for such a model is a knowledge of the thermal conductivity of soils at high temperature. The purpose of this paper is to present measurements of thermal conductivity under high temperature conditions relevant to burning, and to compare the measurements to predictions from a model.

Materials and Methods

Thermal conductivity was measured on samples from nine soils and from peat moss. Table 1 lists the soils and indicates their origin. Samples were dried to air dryness and the soils were passed through a 2 mm sieve. Measurements were made only on the sieved fractions. Thermal conductivity measurements were made using the method and analysis described by Shiozawa and Campbell (1990). Heated probes (Soiltronics, 1111 Myrtle Dr., Burlington, WA 98233) 0.9 mm diameter x 40 mm long, were mounted axially in 4.3 cm diameter x 4.3 cm long pieces of plastic pipe. Soil samples were moistened to predetermined water contents, mixed, and packed to uniform bulk density in the pipes. The pipes were were then covered, sealed with tape, and placed in a controlled temperature oven for measurement. Measurements were taken at 4 sample temperatures: 30, 50, 70 and 90 C using a microprocessor controlled data logger (Model CR7X, Campbell Scientific, Inc., Logan, UT 84321). Equilibration took approximately 6 hours at each temperature. Measurements always proceeded from cold to hot. Measurements over a range of bulk

densities and water content were made on each sample. The Marquardt (1963) non-linear least squares algorithm, as given by Shiozawa and Campbell (1990), was used to determine thermal conductivity from each set of measurements.

Prediction of Thermal Conductivity

The model used to predict thermal conductivity of soils at high temperatures is similar to that of de Vries (1963). It is based on the assumption that the thermal conductivity of any mixture can be expressed as the weighted sum of the thermal conductivities of the components of the mixture. If we consider soil to be a mixture of water, gas and mineral, having volume fractions, x_w, x_a and x_m, with thermal conductivities, λ_w, λ_a and λ_m, then the overall thermal conductivity of the soil can be expressed as

$$\lambda = \frac{k_w x_w \lambda_w + k_a x_a \lambda_a + k_m x_m \lambda_m}{k_w x_w + k_a x_a + k_m x_m} \quad (1)$$

The thermal conductivity of the gas phase, λ_a, is considered to be an apparent thermal conductivity, which is the sum of the actual conduction through the air, and the latent heat of distillation across pores in the soil. The variation of the latent heat term with temperature is the primary factor responsible for temperature dependence of thermal conductivity in soil.

The k's in eq. (1) are the weighting factors. They are, to a large extent, empirically determined in the de Vries theory, and are the most difficult part of the theory to deal with. de Vries used different models to calculate the k's, depending on which phase (gas or water) he considered to be continuous, and then interpolated between the results to obtain a continuous function over the full range of soil water content. In an effort to reduce some of the subjectivity and complexity of this approach, we defined a continuous function for k which applies over the full range of water contents. This was done by first defining a "fluid" thermal conductivity:

$$\lambda_f = \lambda_a + f_w(\lambda_w - \lambda_a) \quad (2)$$

where f_w is an empirical weighting function given by

$$f_w = 1/[1+(x_w/x_{wo})^{-q}] \quad (3)$$

which ranges from 0, in dry soil, to 1 in saturated soil. The parameters, x_{wo} and q are soil properties which relate to the water content at which water starts to affect thermal conductivity and the rapidity of the transition from

air to water-dominated conductivity. We found that q is temperature dependent, and described the temperature dependence as

$$q = q_o(\Theta/303)^2 \quad (4)$$

where q_o is constant, and Θ is the kelvin temperature of the soil.

Using eq. (2), the weighting factors then become:

$$k_a = \{2/[1+(\lambda_a/\lambda_f-1)g_a]+1/[1+(\lambda_a/\lambda_f-1)g_c]\}/3 \quad (5)$$

$$k_w = \{2/[1+(\lambda_w/\lambda_f-1)g_a]+1/[1+(\lambda_w/\lambda_f-1)g_c]\}/3 \quad (6)$$

$$k_m = \{2/[1+(\lambda_m/\lambda_f-1)g_a]+1/[1+(\lambda_m/\lambda_f-1)g_c]\}/3 \quad (7)$$

where g_a and g_c are shape factors, as described by de Vries (1963). We used the relationship from de Vries: $g_c=1-2g_a$, and took g_a as a constant fitting factor to be determined empirically. The value chosen has little effect, except in dry soil, so g_a became the parameter that allowed accurate prediction of thermal conductivity of the dry soil.

The thermal conductivity of the mineral fraction was assumed to be independent of temperature, but the thermal conductivity of water and dry air were adjusted for temperature using handbook data. A quadratic fit to the data gives:

$$\lambda_w = 0.554 + 2.24 \times 10^{-3}T - 9.87 \times 10^{-6}T^2 \quad (8)$$

$$\lambda_{da} = 0.024 + 7.73 \times 10^{-5}T - 2.6 \times 10^{-8}T^2 \ . \quad (9)$$

The apparent thermal conductivity of air, λ_a, is the sum of the dry conductivity and a vapor term due to latent heat transfer, λ_v. For a saturated pore, de Vries (1963) shows the vapor term to be:

$$\lambda_v^s = H_v\hat{\rho}D_v s/(P-p^*) \ . \quad (10)$$

H_v is the latent heat of vaporization of water, $\hat{\rho}$ is the molar density of air (mol m^{-3}), D_v is the vapor diffusivity in air, P is atmospheric pressure, p^* is the (saturation) vapor pressure of water in the pore, and s is the slope of the saturation vapor pressure vs temperature function. The term $1/(P-p)$ is a mass flow factor which accounts for the increase in mass of gas at the evaporating surface and the consequent drift of the bulk gas phase away from the surface when evaporation occurs.

The terms in eq (10) which have a strong temperature dependence are $\hat{\rho}_a$, D_v, s and p^*. In addition, both $\hat{\rho}$ and D_v have a pressure dependence. The following equations were used to evaluate these terms:

$\hat{\rho} = \hat{\rho}_o(P/P_o)(\Theta_o/\Theta)$ (mol m^{-3})

$D_v = D_{vo}(P_o/P)(\Theta/\Theta_o)^{1.75}$ (m^2 s^{-1})

$p^* = 101325\ exp(13.3016t-2.042t^2+ 0.26t^3 + 2.69t^4)$ (Pa)

$s = 373.15\ p^*(13.3015-4.082t+0.78t^2+10.76t^3)/\Theta^2$ (Pa/K)

where $t = 1-373.15/\Theta$, a dimensionless temperature, $\Theta = T + 273.16$, is the Kelvin temperature, P_o is sea-level pressure, and Θ_o is 273.15 K. We followed Fuller et al. (1966) and used 1.75 as the power of the temperature function in the diffusivity equation, rather than 2.3 as de Vries used. The 1.75 value appears to be based on more extensive measurements. The equation for p^* is from Richards (1971), and the equation for the slope is just $dp^*/d\Theta$. Standard values for density and diffusivity were defined at 0 C and sea level pressure. These are $\hat{\rho}_o = 44.65$ mol m^{-3} and $D_o = 2.12 \times 10^{-5}$ m^2 s^{-1}. The temperature dependence of latent heat of vaporization was approximated by a linear equation:

$H_v = 45144 - 48\ T$ (J/mol).

As the water content of the soil decreases, the latent heat transport across pores decreases. Two factors account for this decrease. First, the humidity in the pore decreases due to a lowering of the water potential in the soil. This has the effect of decreasing s to a value of hs, and decreasing the mass flow factor to a value of $1/(P-hp^*)$. The second factor has to do with liquid movement in the soil. Latent heat transport is strongly dependent on the ability of the pore to recirculate the evaporated water. When the hydraulic conductivity of the pore walls becomes low enough to impede return liquid flow within the pore, the latent heat term begins to decrease. Both factors are taken into account in the following expression for vapor conductivity:

$$\lambda_a = H_v h f_w \hat{\rho} D_v s/(P-hp^*) \qquad (11)$$

where h is the relative humidity and f_w is from eq. (3). In practice, f_w starts to decrease well before h, as water content decreases, so h never limits latent heat transfer, and can be set to unity.

This model explicitly accounts for variation in thermal conductivity due to temperature, bulk density and soil water content. Only four parameters are needed to predict thermal conductivity. These are the thermal conductivity of the mineral fraction, λ_m, the water content for liquid transport, x_{wo}, the power for the liquid transport function, q_o, and the shape factor, g_a. The thermal conductivity of dry soil tends to be controlled by g_a, the conductivity of wet soil by λ_m, and the transition point by x_{wo}. Ideally, one

could predict all of these parameters from basic physical properties of the soil so that no fitting of parameters would be necessary.

Results and Discussion

The measured values of thermal conductivity for the ten samples are shown in Fig. 1. Table 1 gives relevant physical properties. The data were collected for a range of bulk densities, as indicated in Table 1. To compare these data on a single graph, the values plotted in Fig. 1 were corrected to the indicated bulk density (the mean of the measured values) using the bulk density dependence of eq. (1).

The 30 C conductivities appear to be most consistent for all samples, and these are least influenced by λ_v, so they were used to determine λ_m, g_a, q_o, and x_{wo} for each sample. These parameters were obtained by non-linear least squares fits, using the Marquardt (1963) procedure, to the 30 C data. The values obtained are shown in Table 1. Regression coefficients and rms errors for the fits are also given. The predictions of the model for 30 C are shown in Fig. 1, and indicate good agreement between model and measured values.

The mineral thermal conductivities (Table 1, λ_m) obtained by fitting the data are consistent with published values. Hodgman et al. give thermal conductivities of basalt, granite, and glass as 2.2, 2.0 and 1.1 W m^{-1} C^{-1}. de Vries gives values for quartz, clay minerals, and organic matter of 8.8, 2.9 and 0.25 W m^{-1} C^{-1}. The L soil, Palouse, Walla Walla and Royal are all loess, derived from basalt parent materials. The Bouldercreek soil is high in volcanic ash, and therefore has a much lower mineral thermal conductivity. The Volkmar soil comes from the Tannana river valley in Alaska. Its mineral conductivity may indicate a higher quartz content than is present in the other soils. The solids conductivity of the peat moss is close to the value for organic matter given by de Vries.

The values for x_{wo} are correlated with soil texture (Fig. 2). The relationship between x_{wo} and geometric mean particle diameter for the 9 samples is

$$x_{wo} = 0.267\ d_g^{-0.2} \qquad (12)$$

where d_g is in μm, and x_{wo} is in m^3 m^{-3}. The fit of eq. (12) to the data is shown in Fig. 2. Values of g_a and q_o also show variation from soil to soil, but we were unable to find any consistent pattern in our data.

Once the model parameters were determined using the 30 C data, the model was used to predict thermal conductivities for the other temperatures. These predictions are also shown in Fig. 1. While some of the data show reasonable agreement with the predictions, some measurements are well below the predicted values. The tendency to under predict appears to increases as temperature increases. In many cases, the predicted values appear to form an upper boundary for the measured values. Since the model is straightforward with respect to prediction of temperature effects on thermal conductivity, our inclination is to doubt the validity of some of the measurements at high temperature.

We tried fitting the model to all of the data, and, of course, obtained better fits to the high temperature thermal conductivity measurements. The mineral conductivities obtained from these fits, however, were considerably lower than the values in Table 1, and were therefore well below measured values for the minerals themselves.

It is possible that liquid return flow becomes limiting at high temperatures because of the increased volume of water that recirculates in a pore. If this were true, however, one would expect the effect to be greatest on the low water content end of the curves and least for the wet soil. The data (Figure 1) do not necessarily show this to be the case. At low water content, measurements and model predictions agree quite well. Also, some measurements do fall near the predictions at higher water contents. We concluded that the model predictions are the most reliable estimates of thermal conductivity at high temperature, and used them in our simulations of heat flow under fires (this report). We found that the simulations were relatively insensitive to the actual values used for moist soil thermal conductivity. We were therefore not able to determine whether the model or the measured conductivities are correct, but found that the modeled values were adequate for simulation purposes.

Summary

Soil thermal conductivity estimates, which are good at low temperature, and adequate for simulations at high temperature, can be obtained using a modification of the de Vries theory of mixtures. Four parameters are required to completely specify thermal conductivity as a function of bulk density,

temperature and water content: thermal conductivity of the mineral fraction, water content at which liquid return flow becomes limiting, a power for the return flow function, and a shape factor. Adequate estimates of the conductivity of the mineral fraction can be obtained from handbooks if the soil mineralogy is known, and the water content for liquid return flow can be predicted from soil texture. The other two parameters show a fairly narrow range of variation, and can probably be estimated with sufficient accuracy for most simulation purposes.

References

de Vries, D. A. 1963. Thermal properties of soils. p. 210-235. In W. R. Van Wijk (ed.) Physics of plant environment. North Holland Pub. Co., Amsterdam.

Fuller, E. N., P. D. Schettler and J. C. Giddings, 1966. A new method for prediction of binary gas-phase diffusion coefficients. Industrial and Engineering Chemistry, 58:19-22.

Hodgman, C. D., R. C. Weast, and S. M. Shelby, eds. 1959. Handbook of Chemistry and Physics, 41st Ed., Chemical Rubber Publishing Co., Cleveland.

Marquardt, D. W. 1963. An algorithm for least-squares estimation of nonlinear parameters. J. Soc. Indust. Appl. Math. 11:431-441.

Richards, J. M. 1971. Simple expression for the saturation vapor pressure of water in the range -50 to 140. Brit. J. Appl Phys. 4:L15-L18.

Shiozawa, S. and G. S. Campbell. 1990. Soil Thermal Conductivity. Remote Sensing Reviews 5:301-310.

Shiozawa, S. and G. S. Campbell. 1991. On the calculation of mean particle diameter and standard deviation from sand, silt and clay fractions. Soil Sci., in press.

Table 1. Thermal and physical properties of soil samples and peat moss. Bulk density (ρ_b) gives the range of bulk densities for the runs shown in Fig. 1. The r^2 and s_{yx} values are for the 30 C fits shown in Fig. 1.

Soil[1]	ρ_b Mg m^{-3}	d_g μm	λ_m W/(mK)	x_{wo} m^{3}m^{-3}	g_a -	q_o -	r^2 -	s_{yx} W/(mK)
L soil	1.15-1.70	188.7	2.61	0.091	0.090	3.01	0.973	0.058
Bouldercreek	0.59-0.86	31.8	1.03	0.133	0.130	6.08	0.998	0.008
Palouse A	1.11-1.52	7.9	2.31	0.148	0.071	4.14	0.996	0.026
Palouse B	1.86-1.38	1.9	2.00	0.230	0.074	5.83	0.986	0.026
Salkum	0.99-1.31	7.9	2.21	0.152	0.084	4.63	0.978	0.050
Walla Walla	0.94-1.52	15.4	2.53	0.218	0.103	3.43	0.986	0.056
Royal	1.09-1.51	23.6	2.57	0.127	0.106	2.93	0.987	0.051
Volkmar	1.27-1.69	71.5	4.71	0.150	0.116	1.71	0.990	0.066
Mokins	0.94-1.47	6.9	2.64	0.209	0.071	3.62	0.970	0.075
Peat moss	0.14-0.18		0.29	0.170	0.330	1.97	0.997	0.005

[1]Soil descriptions are

L-soil: Mixture of Quincy sand and subsoil; mixed mesic Xeric Torripsamments from Hanford nuclear reservation in Central Washington.

Bouldercreek: Medial over loamy-skeletal, mixed frigid Typic Vitrandepts from mountains near Wallace, ID.

Palouse: Fine-silty, mixed, mesic Pachic Ultic Haploxeroll from Witman County, WA.

Salkum: Fine, mixed, mesic Ultic Haploxeralf from Lewis County, WA.

Walla Walla: Coarse-silty, mixed, mesic Typic Haploxeroll from Adams County, WA.

Royal: Coarse-loamy, mixed, mesic Xerollic Camborthids from Franklin County, WA.

Volkmar: Aeric Cryaquept from Delta, Alaska.

Mokins: Silt loam from Kootenai County, ID.

Figure Captions

Figure 1. Thermal conductivity of soil samples as a function of volume fraction of water and temperature. Points are measured values, lines are predictions from the modified de Vries theory. Filled squares are 30 C, empty squares are 50 C, filled triangles are 70 C, and squires with x are 90 C.

Figure 2. Limiting water content for return flow as a function of geometric mean particle diameter.

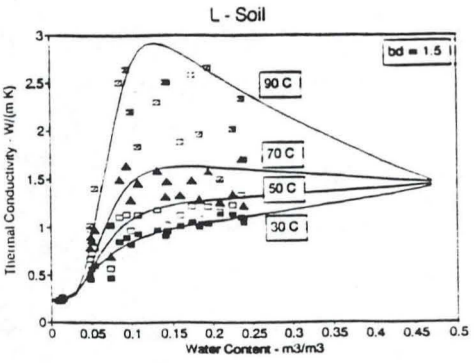
L - Soil
bd = 1.5
90 C
70 C
50 C
30 C
Thermal Conductivity - W/(m K)
Water Content - m3/m3

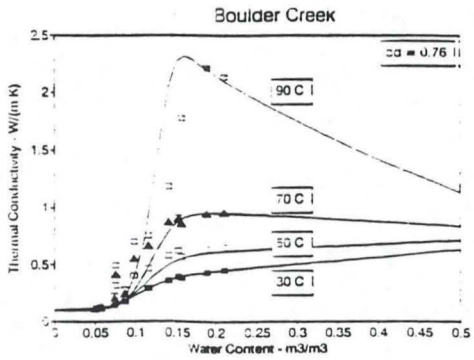
Boulder Creek
bd = 0.76
90 C
70 C
50 C
30 C
Thermal Conductivity - W/(m K)
Water Content - m3/m3

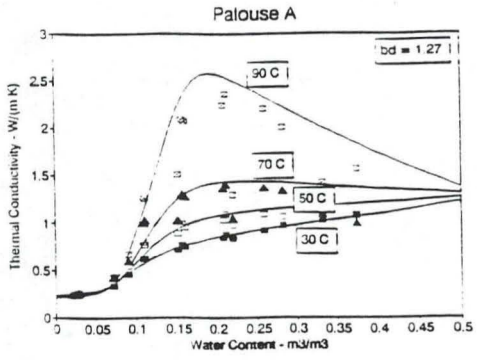
Palouse A
bd = 1.27
90 C
70 C
50 C
30 C
Thermal Conductivity - W/(m K)
Water Content - m3/m3

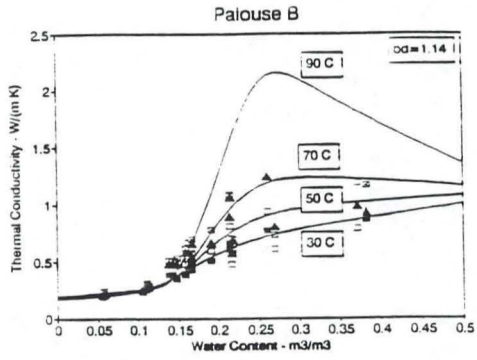
Palouse B
bd=1.14
90 C
70 C
50 C
30 C
Thermal Conductivity - W/(m K)
Water Content - m3/m3

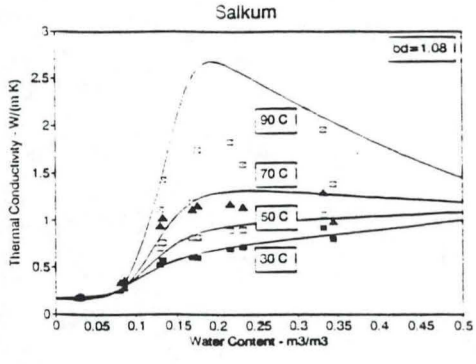
Salkum
bd=1.08
90 C
70 C
50 C
30 C
Thermal Conductivity - W/(m K)
Water Content - m3/m3

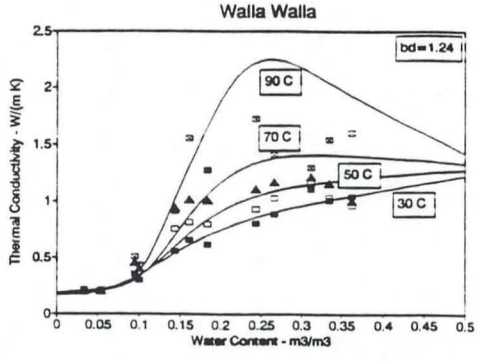
Walla Walla
bd=1.24
90 C
70 C
50 C
30 C
Thermal Conductivity - W/(m K)
Water Content - m3/m3

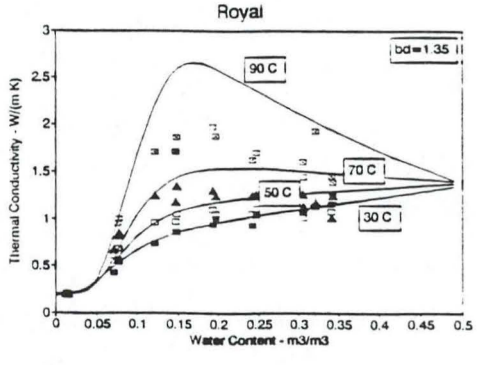
Royal
bd=1.35
90 C
70 C
50 C
30 C
Thermal Conductivity - W/(m K)
Water Content - m3/m3

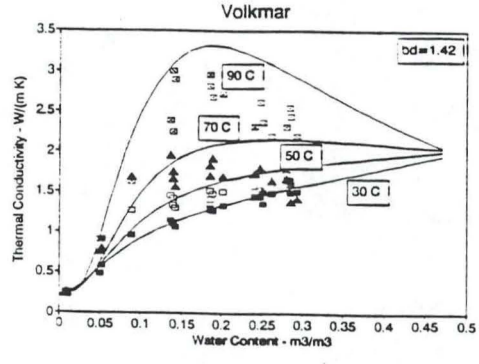
Volkmar
bd=1.42
90 C
70 C
50 C
30 C
Thermal Conductivity - W/(m K)
Water Content - m3/m3

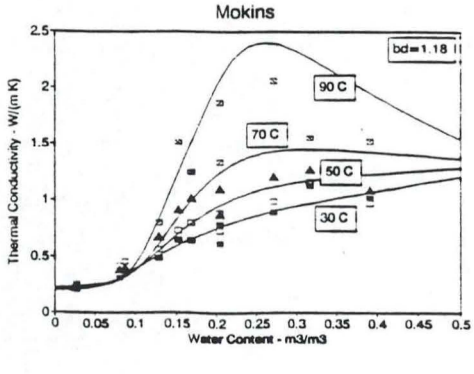
Mokins
bd=1.18
90 C
70 C
50 C
30 C
Thermal Conductivity - W/(m K)
Water Content - m3/m3

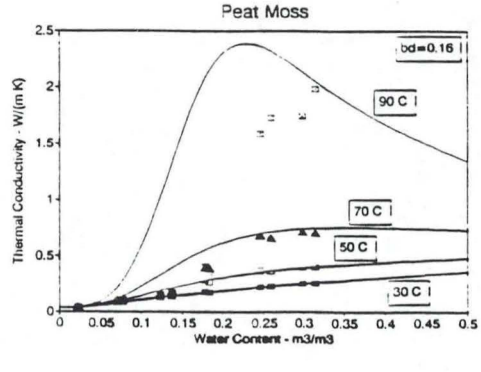
Peat Moss
bd=0.16
90 C
70 C
50 C
30 C
Thermal Conductivity - W/(m K)
Water Content - m3/m3

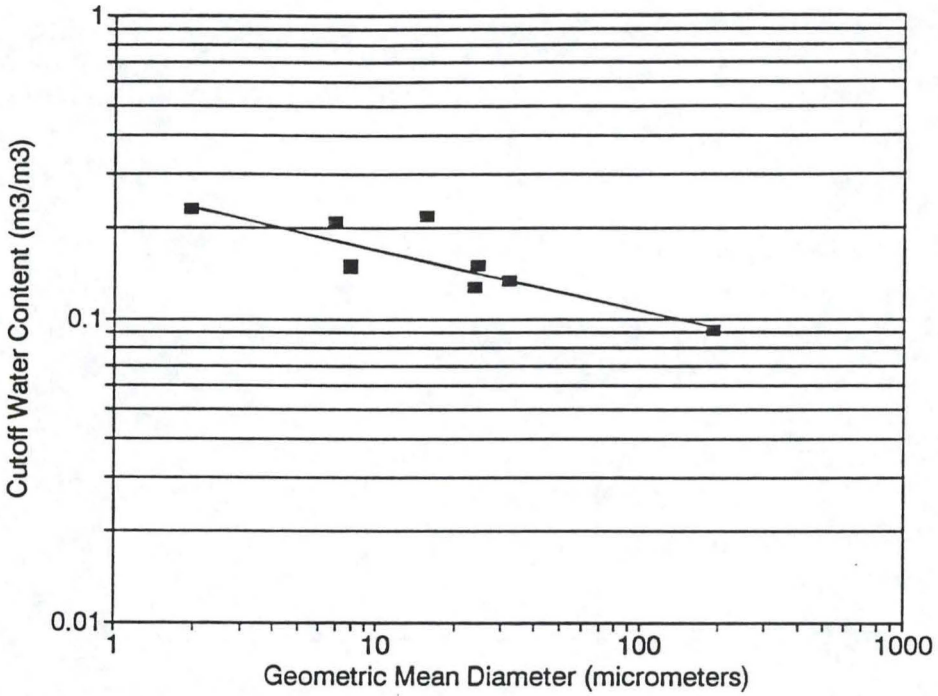
1
0.1
0.01
Cutoff Water Content (m3/m3)
1
10
100
1000
Geometric Mean Diameter (micrometers)

A One-Parameter Equation for Sorption Isotherms in Soils

G. S. Campbell, J. D. Jungbauer, Jr., S. Shiozawa and R. D. Hungerford

Introduction

In order to model the drying of soil as it heats under a fire, it is necessary to know the relationship between the water activity or equilibrium relative humidity of the soil water and the water content of the soil. We report here on the performance of a simple, single-parameter model which describes this relationship.

Models

The usual model used to describe sorption isotherms for soils was suggested by Fink and Jackson (1973):

$$h = [1 + (w/a)^{-b}]^{-c} \quad (1)$$

where h is humidity or water activity, w is water content (g/g), and a, b, and c are empirical constants to be determined from data.

Our new single-parameter model is based on the moisture release curve of Campbell and Shiozawa (1991). They found a simple linear relationship between water content and the logarithm of the water potential:

$$w = w_1[1-ln(-\psi)/ln(-\psi_o)] \quad (2)$$

where w_1 is the extrapolated value of the water content when ψ = -1 J/kg, and ψ_o is the water potential of oven dry soil (-10^6 J/kg). Water potential and humidity are related using the thermodynamic equation:

$$\psi = (RT/M_w)\ ln(h) \quad (3)$$

where R is the gas constant, T is absolute temperature, and M_w is the molecular mass of water. Combining eqs. (2) and (3) gives

$$h = exp\{(M_w/RT)exp[(1-w/w_1)ln(-\psi_o)]\} \quad (4)$$

The only free parameter in eq. (4) is w_1.

Materials and Methods

Water activity measurements on nine soils and peat moss were used to compare the two sorption equations. Data on six of the soils were available from the work of Campbell and Shiozawa (1991). These data were obtained by pressure plate, thermocouple psychrometer, and water activity meter (described

below), but most were from the water activity meter. Measurements on three additional soils, and on peat moss were made by mixing water with dry soil to obtain water activities in the range, 0.1 to 1.0. Samples were sealed in aluminum cans and allowed to equilibrate overnight to ensure uniformity. Measurements were made using a dew point-type water activity meter (model CX-1, Decagon Devices, Inc., P.O. Box 835, Pullman, WA 99163). Three measurements were taken for each of six samples. The average of the three readings was reported as the water activity value. Samples were then oven dried to obtain the water content. Models were fit to the data using a non-linear least squares procedure (Marquardt, 1963)

Results and Discussion

Figure 1 shows typical fits of the two equations to the data for two of the soils. It appears that eq. (4) may underestimate the correct water activity at high water activities in the sandy L-soil. On the other hand, eq. (4) may fit slightly better at low water activity in the high-clay Palouse-B samples. Both models fit the data well, and should be adequate for modeling soil drying.

Table 1 shows the results for all ten samples. In eight of the ten cases, there appears to be little difference between the quality of the fits obtained with eq. (4) and those obtained with eq. (1), even though eq. (4) has two fewer parameters. In the case of the Volkmar soil, the water contents were so low that their uncertainty may have contributed substantially to the error. The additional parameters in eq. (1) may have been just fitting the "noise" in the measurements, since there were so few data points. On the other hand, the fit to the peat moss data was clearly poorer with eq. (4), and it appears that the more complex equation is needed to fit these data.

Campbell and Shiozawa (1991) showed that the single parameter, w_1, in eq. (4) is strongly correlated with clay content and specific surface of the soil. It is therefore easily predicted from texture. An even simpler method for predicting its value, however, is the use the air dry water content of the sample. Solving eq. (2) for w_1 gives

$$w_1 = w_a/[1-ln(-\psi_a)/ln(-\psi_o)] \qquad (5)$$

where w_a is the air dry water content and ψ_a is the water potential. If the

average humidity of the laboratory in which the soil is air-dried is 0.5, then, using eq. (3), $\psi_a \cong -10^5$ J/kg. Substituting into eq. (5) gives $w_1 = 6w_a$. The relationship between $w1$ and w_a is shown in Fig. 2 for the nine mineral soil samples. While there is some scatter, possibly due to uncertainty in ψ_a (the samples were equilibrated in a laboratory without humidity control), the correlation is still high between the variables. Regression analysis gave $w_1 = 6.2\ w_a$, with $r^2 = 0.76$.

Summary

Our simple equation for predicting water activity in dry soils has several advantages over the Fink-Jackson model. The most important is that it requires only a single parameter, which can be estimated from texture data or from a measurement of air dry water content. A more precise value can be obtained from a single water activity measurement. The three parameter model requires several accurate measurements of water activity and water content to determine the parameters. A second advantage is that the simple model is somewhat faster to compute (two exponentials, rather than two logs and two exponentials) so some computer time is saved in complex models. A third advantage is that the simple model readily extends to water contents below oven dryness, while the three-parameter model will not work for negative water contents. This is important in modeling fire conditions where soil temperatures are often above standard oven temperature, giving rise to negative water contents. Because of these factors, we recommend using the simple model to describe the humidity-water content relationship for mineral soils.

References

Campbell, G. S. and S. Shiozawa. 1991. Prediction of hydraulic properties of soils using particle size distribution and bulk density data. Proceedings of a workshop "Indirect Methods for Estimating the Hydraulic Properties of Unsaturated Soils", U. S. Salinity Lab., Riverside, CA.

Fink, D. H. and R. D. Jackson. 1973. An equation for describing water vapor adsorption isotherms of soils. Soil Sci. 116:256-261.

Table 1. Results of fitting eq. (1) and eq.(4) to h vs w data. The s_{yx} values are the uncertainties in the predicted humidities.

	--------Fink - Jackson--------					------Eq. (4)------		
Soil[1]	a	b	c	r^2	s_{yx}	w_1	r^2	s_{yx}
L soil	0.016	11.7	0.168	0.995	0.026	0.064	0.989	0.036
Bouldercreek	0.088	21.3	0.079	0.976	0.059	0.321	0.944	0.070
Palouse A	0.053	5.65	0.319	0.997	0.019	0.207	0.995	0.022
Palouse B	0.094	5.92	0.316	0.997	0.018	0.373	0.996	0.021
Salkum	0.039	3.78	0.727	0.998	0.017	0.202	0.998	0.016
Walla Walla	0.037	4.35	0.443	0.996	0.021	0.157	0.995	0.024
Royal	0.024	4.96	0.413	0.995	0.025	0.102	0.995	0.025
Volkmar	0.017	6.27	0.193	0.989	0.040	0.054	0.934	0.077
Mokins	0.031	3.33	0.722	0.998	0.019	0.156	0.990	0.031
Peat moss	0.227	3.64	0.298	0.997	0.023	0.744	0.906	0.094

[1]Soil descriptions are

L-soil: Mixture of Quincy sand and subsoil; mixed mesic Xeric Torripsamments from Hanford nuclear reservation in Central Washington.

Bouldercreek: Medial over loamy-skeletal, mixed frigid Typic Vitrandepts from mountains near Wallace, ID.

Palouse: Fine-silty, mixed, mesic Pachic Ultic Haploxeroll from Witman County, WA.

Salkum: Fine, mixed, mesic Ultic Haploxeralf from Lewis County, WA.

Walla Walla: Coarse-silty, mixed, mesic Typic Haploxeroll from Adams County, WA.

Royal: Coarse-loamy, mixed, mesic Xerollic Camborthids from Franklin County, WA.

Volkmar: Aeric Cryaquept from Delta, Alaska.

Mokins: Silt loam from Kootenai County, ID.

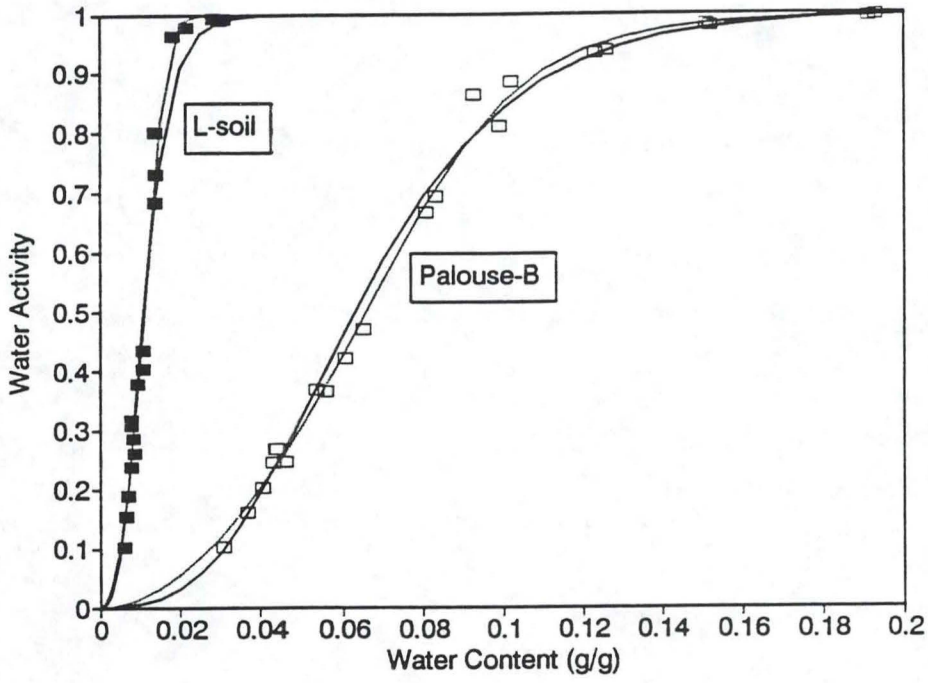

Figure 1. Example fits of water activity - water content data. The solid line is eq. (4); the dashed line is the Fink-Jackson equation (eq. 1).

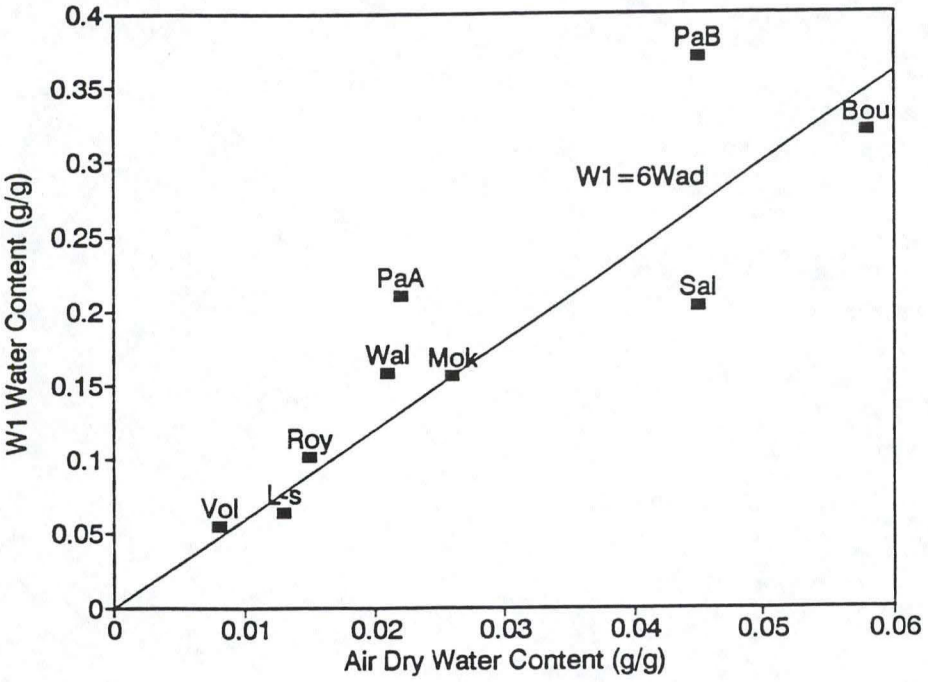

Figure 2. Relationship between the w_1 parameter, as determined from fits to moisture release data, and air dry water content.

Thermal Properties of Duff Layers

James D. Jungbauer, Jr.

Introduction

Heat transfer through organic layers at the soil surface can have an important influence on the soil temperatures under fires. It is therefore important to know what the thermal properties of those layers are. This report describes measurements which were made on six samples of duff taken from the surfaces of soils in forested areas.

Materials and Methods

Thermal conductivity measurements were taken on six different organic layer samples provided by the USFS Fire Lab in Missoula, MT. The block-shaped samples varied slightly in size, but all were approximately 7-9 cm high, and 19-23 cm long on both sides. Detailed descriptions, provided by the Fire Lab, are attached. Measurements were taken both when the blocks were wet and when they were air-dry, and over a range of temperatures. However, only samples 5 and 8 were examined through the entire range of temperatures under both wet and dry conditions; samples 1, 2, 4, and 7 were measured at varying temperatures only while they were wet. The air-dry measurements on these last four were taken only at room temperature because, as temperature changed, no significant changes in thermal conductivity were observed in samples 5 and 8 while air-dry (there were also no real differences between thermal conductivity values for any of the ten samples while air-dry).

All measurements were made using thermal conductivity probes (Decagon Devices, Inc., P.O. Box 835, Pullman, WA 99163), which measure 14.5 cm in length. Each probe consists of a heating element and a thermocouple embedded in an epoxy-filled piece of stainless steel tubing (1.27 mm outside diameter). The heating element wire is connected through a 10 ohm reference resistor. The wires from the element and the thermocouple were connected to a power supply and a recording channel, respectively, on a microprocessor-controlled datalogger (model CR7X, Campbell Scientific, Inc., Logan, UT 84321).

In preparation for the measurements on wet samples, the blocks were placed in a shallow pan of water, covered with plastic, and allowed to sit for several days so that all of the water was absorbed and distributed evenly throughout the sample. After they were prepared, three thermal conductivity

probes were inserted horizontally into each block: one into the top, vegetation-dominant layer, another into the middle, partially decayed layer, and the third into the lowest, most solid layer which contained the least non-soil material. The probes were spaced apart laterally so that probes in adjacent layers would not affect each other's readings. The blocks were then put into plastic bags, leaving only an opening for the thermal conductivity probe wires which were connected to the datalogger. The bags were sealed around these wires in two places so that no water could escape. The sealed blocks were then put into an oven, which was also controlled by the datalogger.

Measurements were taken at four different temperatures: 30°C, 50°C, 70°C, and 90°C. For each one, the oven was set to the appropriate temperature, and the samples were given six hours to equilibrate at that temperature before measurements began. (In earlier experiments, six hours had proven to be sufficient to stabilize the samples at any of these temperatures and at the necessary water contents). After the six hours had passed, the oven was turned off and a voltage (enough to cause a temperature rise of at least one to three degrees C) was applied to the heaters inside the probes. Temperatures from the thermocouples within the probes were recorded every second for 100 seconds while the probes heated. Then the heaters were turned off and temperatures were again recorded every second for 100 seconds while the probes cooled. The voltage applied to the heaters was also recorded every second so that an average power could be calculated. Equation (8) of Jackson and Taylor (1986) was fit to the temperature data by non-linear least squares (Marquardt, 1963) to obtain thermal conductivity. Shiozawa and Campbell (199) give a computer program for making the calculations.

After completing readings at all four temperatures on wet samples, the blocks were removed from their bags, and the three layers in each were separated. Each layer was then weighed, and their volumes were determined using water displacement. This involved putting the layer into a flexible plastic bag and submerging it in water inside a measuring cylinder, the cross-sectional area of which was known. The water pressure forced the bag to cling tightly to the layer, and the difference in the water surface level before and after submersion was used to calculate the volume of the layer. The layers were then left to air dry for several days, after which they were

weighed again. From these weights and volumes, the volumetric water contents and bulk densities were determined.

Results and discussion

The results of the thermal conductivity measurements for the heating cycles, along with the volumetric water contents and bulk densities for each layer, are given in Tables 1-6. Water contents for samples 5 and 8 are based on 0% at 60°C dryness, while those for samples 1, 2, 4, and 7 are based on 0% at air dryness. The samples were not dried at 105°C because at that temperature some of the organic material itself may have been destroyed.

As expected, thermal conductivity increased with water content, and with temperature among the wet samples. As noted earlier, temperature had no effect on thermal conductivity when the samples were air-dry. For every sample, the top layer had the lowest bulk density and the bottom layer had the highest bulk density. Thermal conductivity tended to increase with bulk density, with higher values for the bottom layers and lower values for the top layers (of course, water content also increased with bulk density, so both could be factors). There was variation between samples, however, with respect to the relationship between layer and thermal conductivity. For example, samples 1, 2, and 5 did not follow this pattern as strongly as did the others, and in particular, the bottom layer of sample 2 showed unusually low thermal conductivity values at all temperatures while wet.

There was also some variation between samples in the overall thermal conductivity values, with maximums for individual samples ranging from 1.0 to 1.8. For example, the value for the bottom layer of sample 8 at 90°C is 1.25 while the same layer in samples 1 and 4 at 90°C has values of 1.77 and 1.70, respectively, even at lower water contents (although at higher bulk density). Meanwhile, the bottom layer of sample 7 at 90°C has a value of 0.85 at a slightly lower water content but much higher bulk density.

While there is substantial variation in the thermal conductivities we measured, the results generally seem consistent with the measurements and model predictions for peat moss given by Campbell et al (this report, thermal conductivity). The large variation encountered is likely due to the lack of homogeneity of the samples. The thermocouple of the conductivity probe could easily come into contact with a twig or large air gap, as it is inserted, and

these would give quite different readings for the same material. We therefore feel that the most representative value for the thermal conductivity will be the one predicted by the model for the density and water content of the organic layer.

References

Jackson, R. D. and S. A. Taylor. 1986. Thermal conductivity and diffusivity p. 945-956. In Methods of Soil Analysis, Part 1. Physical and Mineralogical Methods, A. Klute (ed.). Agronomy Monographs no. 9 (2nd Edition). American Society of Agronomy, Madison, WI.

Marquardt, D. W. 1963. An algorithm for least-squares estimation of nonlinear parameters. J. Soc. Indust. Appl. Math. 11:431-441.

Shiozawa, S. and G. S. Campbell. 1990. Soil Thermal Conductivity. Remote Sensing Reviews 5:301-310.

Table 1. Sample 5 Results

layer	temp. (C)	water content (g/cc)	bulk density (g/cc)	thermal cond. (W/m/K)
top	30	0.00	0.12	0.0382
	50	0.00	0.12	0.0435
	70	0.00	0.12	0.0480
	90	0.00	0.12	0.0473
	30	0.20	0.12	0.2113
	50	0.20	0.12	0.2893
	70	0.20	0.12	0.3443
	90	0.20	0.12	0.7046
middle	30	0.00	0.14	0.0497
	50	0.00	0.14	0.0579
	70	0.00	0.14	0.0640
	90	0.00	0.14	0.0629
	30	0.32	0.14	0.2264
	50	0.32	0.14	0.2439
	70	0.32	0.14	0.4211
	90	0.32	0.14	0.4946
bottom	30	0.00	0.19	0.0464
	50	0.00	0.19	0.0526
	70	0.00	0.19	0.0587
	90	0.00	0.19	0.0588
	30	0.37	0.19	0.2944
	50	0.37	0.19	0.3852
	70	0.37	0.19	0.6057
	90	0.37	0.19	1.5548

Table 2. Sample 8 Results

layer	temp. (C)	water content (g/cc)	bulk density (g/cc)	thermal cond. (W/m/K)
top	30	0.00	0.06	0.0232
	50	0.00	0.06	0.0266
	70	0.00	0.06	0.0289
	90	0.00	0.06	0.0288
	30	0.09	0.06	0.1016
	50	0.09	0.06	0.1785
	70	0.09	0.06	0.3409
	90	0.09	0.06	0.3627
middle	30	0.00	0.12	0.0357
	50	0.00	0.12	0.0410
	70	0.00	0.12	0.0435
	90	0.00	0.12	0.0411
	30	0.21	0.12	0.2451
	50	0.21	0.12	0.3671
	70	0.21	0.12	0.6223
	90	0.21	0.12	0.5819
bottom	30	0.00	0.33	0.0877
	50	0.00	0.33	0.0923
	70	0.00	0.33	0.0966
	90	0.00	0.33	0.0952
	30	0.32	0.33	0.5775
	50	0.32	0.33	0.6716
	70	0.32	0.33	0.9045
	90	0.32	0.33	1.2501

Table 3. Sample 1 Results

layer	temp. (C)	water content (g/cc)	bulk density (g/cc)	thermal cond. (W/m/K)
top	20	0.00	0.09	0.0222
	30	0.11	0.09	0.2561
	50	0.11	0.09	0.3843
	70	0.11	0.09	0.6576
	90	0.11	0.09	1.5773
middle	20	0.00	0.24	0.0291
	30	0.25	0.24	0.6800
	50	0.25	0.24	0.6766
	70	0.25	0.24	0.7699
	90	0.25	0.24	1.0829
bottom	20	0.00	0.44	0.0677
	30	0.29	0.44	0.2665
	50	0.29	0.44	0.5725
	70	0.29	0.44	0.7928
	90	0.29	0.44	1.7708

Table 4. Sample 2 Results

layer	temp. (C)	water content (g/cc)	bulk density (g/cc)	thermal cond. (W/m/K)
top	20	0.00	0.09	0.0327
	30	0.12	0.09	0.2667
	50	0.12	0.09	0.3910
	70	0.12	0.09	0.6854
	90	0.12	0.09	1.6022
middle	20	0.00	0.25	0.0332
	30	0.29	0.25	0.5428
	50	0.29	0.25	0.5247
	70	0.29	0.25	0.7351
	90	0.29	0.25	1.1783
bottom	20	0.00	0.49	0.0912
	30	0.38	0.49	0.0518
	50	0.38	0.49	0.0567
	70	0.38	0.49	0.0762
	90	0.38	0.49	0.1900

Table 5. Sample 4 Results

layer	temp. (C)	water content (g/cc)	bulk density (g/cc)	thermal cond. (W/m/K)
top	20	0.00	0.07	0.0198
	30	0.15	0.07	0.1359
	50	0.15	0.07	0.1864
	70	0.15	0.07	0.3787
	90	0.15	0.07	0.4921
middle	20	0.00	0.13	0.0413
	30	0.30	0.13	0.4429
	50	0.30	0.13	0.6259
	70	0.30	0.13	0.5152
	90	0.30	0.13	0.5245
bottom	20	0.00	0.46	0.0822
	30	0.31	0.46	0.5529
	50	0.31	0.46	0.7646
	70	0.31	0.46	1.0873
	90	0.31	0.46	1.6967

Table 6. Sample 7 Results

layer	temp. (C)	water content (g/cc)	bulk density (g/cc)	thermal cond. (W/m/K)
top	20	0.00	0.08	0.0215
	30	0.10	0.08	0.0354
	50	0.10	0.08	0.0714
	70	0.10	0.08	0.0750
	90	0.10	0.08	0.0973
middle	20	0.00	0.13	0.0218
	30	0.21	0.13	0.1265
	50	0.21	0.13	0.2701
	70	0.21	0.13	0.2514
	90	0.21	0.13	0.3582
bottom	20	0.00	0.71	0.0570
	30	0.27	0.71	0.6288
	50	0.27	0.71	0.6749
	70	0.27	0.71	1.0438
	90	0.27	0.71	0.8490

DUFF SAMPLE INFORMATION

Sample No. 1

LOCATION: Legal: T 16N R 23W S 17

Aspect N Slope 5% Elevation _____

Slope Position basin Slope Shape concave

VEGETATION: Habitat Type GF/Vagl ?

Cover: Species GF, DF, LPP, WL, PP % 80

Understory species VAGL, BERE, XETE, CACA

4-5.5cm thick

DUFF CHARACTER: Depth 2"? Structure Litter, humus

Remarks: Soil very dry, duff remains intact

DUFF SAMPLE INFORMATION

Sample No. _____

LOCATION: Legal: T _____ R _____ S _____

Aspect _____ Slope _____ Elevation _____

Slope Position _____ Slope Shape _____

VEGETATION: Habitat Type _____

Cover: Species _____ % _____

Understory species _____

DUFF CHARACTER: Depth _____ Structure _____

Remarks:

DUFF SAMPLE INFORMATION

Sample No. 2

LOCATION: West Ninemile Legal: T 16N R 24W S 13

Aspect N Slope 5-0% Elevation

Slope Position ~~At Ridge~~ Ridge Slope Shape 5-0% Convex

VEGETATION: Habitat Type GF- Libo

Cover: Species DF, LPP %

Understory species GF, Libo, ~~X~~ete, Ceru

DUFF CHARACTER: Depth (2") Structure

Remarks: 5-6 cm

1 Sample - Sent to Campbell 12/8/87

DUFF SAMPLE INFORMATION

Sample No. 3

LOCATION: West Ninemile Rd #5520 past 15 mile sign Legal: T 17N R 24W S 29

Aspect N Slope 10 % Elevation

Slope Position mid Slope Shape convex

VEGETATION: Habitat Type

Cover: Species Abla, LPP, GF % 60

Understory species PHAM, XETE,

5-8 cm

DUFF CHARACTER: Depth (2") Structure

Remarks:

1 Sample Keep @ IFSL

DUFF SAMPLE INFORMATION

Sample No. 4

LOCATION: Blue Ninemile part Sample @ 3 mi mark Legal: T 17N R 24W S 20

Aspect N Slope 15 Elevation

Slope Position mid Slope Shape convex

VEGETATION: Habitat Type

Cover: Species LPP, WL; cedar & spruce under % 50

Understory species MEFE, PAMY, VAGL, XETE, CHUM, VIOR, GOOB

5-7 cm

DUFF CHARACTER: Depth (2") Structure

Remarks: 2 full samples plus 1 smaller chunk
1 sample to Campbell 12/8/89
1 @ IFSL

DUFF SAMPLE INFORMATION

Sample No. 5 ?

LOCATION: W. Ninemile # 5520 between mile 1 & 2 Legal: T 17N R 24W S 18

Aspect N Slope 15 Elevation

Slope Position draw Slope Shape concave

VEGETATION: Habitat Type THPL/

Cover: Species WRC, WL, DF, LPP % 80

Understory species GOOS, XETE, Rubus, MOSS

9 - 12cm

DUFF CHARACTER: Depth (6")? Structure

Remarks:

2 samples - 1 is thicker than the other

1 sent to Campbell 12/8/89

1 @ IFSL

DUFF SAMPLE INFORMATION

Sample No. 7

LOCATION: Legal: T 11 N R 22W S 3

Forest Lolo District Missoula

Road No. 451 (1st right) Mile marks etc. @ end of road West Fk Butler Cr.

Aspect S Slope 70% Elevation

Slope Position lower Slope Shape convex

VEGETATION: Habitat Type

Cover: Species PP, DF %25

Understory species Arnv, Carx

DUFF CHARACTER: Depth Structure

Remarks: upslope from road end on ridge; sampled 4 pos. under DF & PP

3 Samples collected (1 is smaller) 1 was sent to Campbell 12/8/89

DUFF SAMPLE INFORMATION

Sample No. 8

LOCATION: Legal: T 11 N R 22W S 3

Forest Lolo District Missoula

Road No. 451 (1st right) Mile marks etc @ rd. end

Aspect N Slope 2 Elevation

Slope Position beach Slope Shape ~~beach~~ convex

VEGETATION: Habitat Type ABGR/VACA ?

Cover: Species LPP, WL; DF, GF, SF %

Understory species Mafo, Vaca, chum, Arnv

DUFF CHARACTER: Depth 4-5 cm 6-8 cm Structure

Remarks: Samples taken across creek up slope from beach (E. of research plot sign) Found very orange soil under 1st, of 3 samples w/ charcoal in soil also

1 sent to Campbell 12/8/89

DUFF SAMPLE INFORMATION

Sample No. ?

LOCATION: Legal: T 11N R 22W S 3

Forest Lolo District Missoula

Road No. 4151 Mile marks etc.

Aspect NW Slope 5-10 Elevation

Slope Position lower Slope Shape

VEGETATION: Habitat Type ABLA /

Cover: Species LPP, WL, DF, SE, Spruce under %

Understory species Meba, Vaca, Chum, Libo

DUFF CHARACTER: Depth 5-7 cm Structure

Remarks: up creek 200+ yards from road and then across creek + up slope about 100 yards
2 samples 1 sent to Campbell 12/8/89
1 @ IFSL

DUFF SAMPLE INFORMATION

Sample No. 10

LOCATION: Legal: T 11N R 22W S 3

Forest Lolo District Missoula

Road No. 4151/1st right Mile marks etc. @ end of road W Fk Butler Cr.

Aspect NW Slope 5° Elevation

Slope Position lower Slope Shape

VEGETATION: Habitat Type

Cover: Species ES, LPP, WL, SE, DF %

Understory species Vaca, Vaca?, Vior, Libo

DUFF CHARACTER: Depth 4.5-6 cm Structure

Remarks: Creek bottom just across creek from end of road
1 sent to Campbell 12/8/89

DUFF SAMPLE INFORMATION

Sample No. 11

LOCATION: Legal: T 13N R 23W S 19

Forest Lolo District Missoula

Road No. Howard Cr. Mile marks etc. 4# near Topo Cr. Rd

Aspect S Slope 0 Elevation

Slope Position bench Slope Shape complex

VEGETATION: Habitat Type Abla/Libo?

Cover: Species LPP seedlings; SF seedlings %

Understory species Libo, Arnu

DUFF CHARACTER: Depth 5cm; 2cm Structure

Remarks: On bench just above Topo Creek Rd junction [illegible] Meadows

3 samples; 2 @ 5cm thick & 1 @ 2cm

Best one sent to Campbell 12/8/89

other @ IFSL

DUFF SAMPLE INFORMATION

Sample No. 12

LOCATION: Legal: T 13N R 24W S 24

Forest Lolo District Missoula

Road No. Howard Cr. Mile marks etc. hairpin turn just past soil [illegible]

Aspect N Slope 40% Elevation

Slope Position lower Slope Shape concave

VEGETATION: Habitat Type

Cover: Species PSme, LPP % [illegible]

Understory species Vagl, XETE, Sbca, ?Out?, Mnfo

DUFF CHARACTER: Depth 2-3 cm Structure

Remarks:

2 samples - much soil also, sample may be thinner

1 to Campbell 12/8/89

1 @ IFSL

Water Loss of Soils at Temperatures Above 105 C

G. S. Campbell and J. D. Jungbauer, Jr.

Introduction

The standard procedure for determining the water content of soils is to weigh the sample, dry the sample at 105 C, and then reweigh to determine the amount of water lost (Gardner, 1986). While it is common knowledge that additional water, and other volatiles, are lost from the soil at higher temperatures, these losses have seldom been quantified.

In soil under fires, temperatures may be several hundred degrees above drying oven temperature. We monitored temperature and water content in soil columns which were heated at the surface with a propane burner, and found that apparent water content (monitored using gamma-ray attenuation) of the surface layers reached values below -0.1 g/g. The purpose of this experiment was to independently measure the changes in apparent water content at high temperature to determine whether the gamma measurements are valid.

We will use the term "apparent" water content to include all of the mass loss that occurs above 105 C. Some of the mass loss, however, is almost certainly from volatilization or oxidation of organic substances in the soil.

Materials and Methods

It was difficult to measure water content in samples removed from the oven and weighed in the usual way, since these extremely dry samples take up water rapidly from the atmosphere as they cool. We therefore devised a counterbalanced beam and load cell to weigh the samples in the kiln. The beam extended through a hole in the wall of the kiln (the kiln was a standard ceramics kiln for baking clay pottery), and a weighing pan was attached to its end inside the oven. A load cell and data logger monitored changes in weight of the contents of the pan with a resolution of about 0.1 g. The data logger also controlled the temperature of the kiln.

Fifty gram samples of air dry soil were placed on the weighing pan, and were monitored as temperature was increased from room temperature to 600 C. The rate of increase was set so that this change took place over a period of about 6 hours. This rate of increase was not slow enough to allow moisture

equilibrium at each temperature, but was intended to simulate the changes in apparent water content which might occur under a fire where conditions are changing fairly rapidly. Comparisons with slower heating rates showed that the final water content reached at 600 C was about the same for the fast and the slow heating rate, but the apparent water content was higher for a given temperature at the high heating rate than at the low. The air dry water content of each of the samples was independently determined through standard oven drying methods.

Results and Discussion

Figure 1 shows a typical drying curve for a soil sample. Mass loss has been converted to water content using the measured sample mass and the air dry water content. The final apparent water content reached is near -0.07. Water content change appears to slow down as the temperature approaches 600 C, but certainly has not stopped. The fact that there is not much change at low temperature is probably because we did not wait for equilibrium, rather than because there was not substantial water to loose at these temperatures.

Table 1 gives the total final water content after kiln-drying and the air dry water contents of the eight samples tested. Figure 2 shows the correlation between the final, kiln dry water content, and the air dry water content. Except for the Walla Walla soil, air dry water content appears to be a good predictor of kiln dry water content. The Walla Walla sample may have had more organic matter than the others, and therefore more loss due to oxidation.

The values in Table 1 are reasonably consistent with the water contents measured by the gamma equipment, except for the Bouldercreek soil. The gamma measurements sometimes reached values about twice as low as those in Table 1 for this soil. Bouldercreek is a soil with high volcanic ash content, which may make it unstable at high temperatures. We do not have any other explanation for its behavior in the gamma equipment.

Conclusion

Apparent water contents well below zero are reached by all soils tested when heated to 600 C. The negative values reached were highly correlated with the air dry water content of the soil, indicating that the surfaces and

mechanisms which bind water at atmospheric humidity and temperature are also probably responsible for binding the water at high temperature. The negative water contents measured by the gamma equipment apparently are correct, with the possible exception of measurements on the Bouldercreek soil.

Reference

Gardner, W. H. 1986. Water Content. p. 493-543 in Methods of Soil Analysis, Part 1. Agronomy Monograph no. 9, American Society of Agronomy, Madison, WI.

Table 1. Air dry and Kiln dry water contents of soil samples. All water contents are relative to 105 C oven dryness.

Soil	air dry g/g	kiln dry g/g
L-soil	0.013	-0.0053
Palouse A	0.022	-0.037
Palouse B	0.045	-0.049
Royal	0.015	-0.022
Walla Walla	0.021	-0.059
Salkum	0.045	-0.059
Volkmar	0.008	-0.021
Bouldercreek	0.058	-0.071

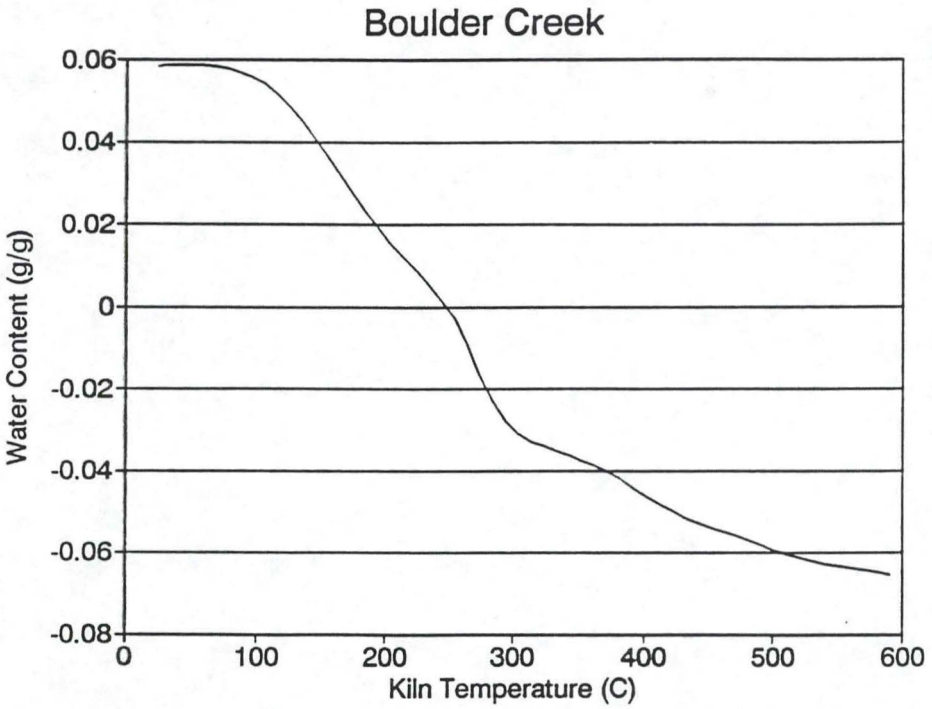

Figure 1. Typical drying curve for Bouldercreek soil in kiln. Water contents are relative to 105 C oven dryness.

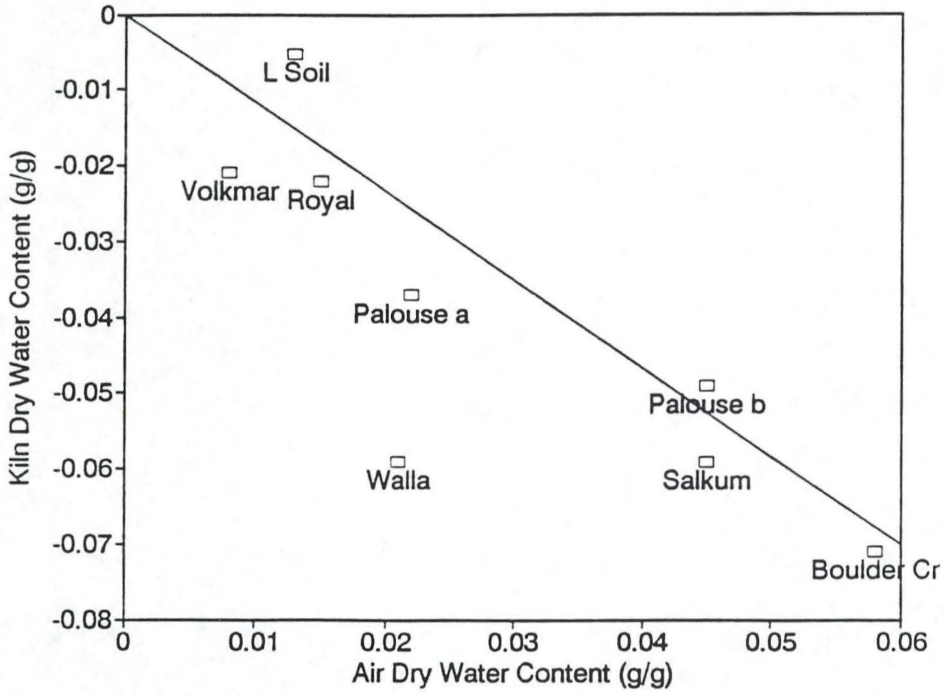

Figure 2. Relationship between apparent kiln dry water content at 600 C and air dry water content. Water contents are relative to 105 C oven dryness.

A Radiometer for Measuring the Flux Density of Radiation Below a Fire

G. S. Campbell

Introduction

In order to model the changes in soil temperature under a fire, it is necessary to know the radiant heat input to the soil surface from the fire. We set up columns in the laboratory to simulate soil heating under fire conditions, and used a propane heater at the surface to simulate the fire. Here we describe a simple radiometer which was used to measure the radiant energy input at the soil surface from the propane heater.

Materials and Methods

The radiometer measured the flux density of radiation by determining the energy absorbed by a 3 cm x 3 cm, blackened copper plate. The temperature rise of water, heated by the plate, was measured to determine the heat absorbed.

Figure 1 shows a diagram of the radiometer. It was constructed inside a 14 cm diam. x 17 cm tall coffee can. The copper sensing plate was soldered to a loop in a piece of 1/4″ copper tubing, which was attached to the inside of the can. The tubing was attached so that the sensing plate was centered, just under the top edge of the can. The can was covered with a circular piece of polished sheet aluminum heat shield with a 3 cm x 3 cm square hole cut at the center, just over the sensing plate. The plate was painted with high-temperature, flat black paint. Copper-constantan thermocouples were soldered to the copper tubing on each side of the sensing plate, so that the temperature of the tubing could be monitored just before and just after the water passed the sensing plate. Thermocouple output was monitored with a data logger (Model 21X, Campbell Scientific, Inc., Logan, UT).

Water flow through the tubing was from a constant-head water supply, consisting of a bubbling tube and a 20 l. plastic jug. The height of the outflow was also kept constant, and was adjusted to give 220 g/min water flow, as measured with a graduated cylinder.

The propane heater was mounted 3.5 cm above the surface of the radiometer; the distance used for the soil column measurements. Measurements were made at both high and low settings of the heater. Temperatures were

monitored until they became stable.

We assumed that conductive heat loss from the sensor plate to the air is negligible, compared to other modes of heat transfer, and that heat gain, by radiation from the propane heater is just balanced by convective heat loss to the water and radiative heat loss.

Results

With the heater on low, the steady temperature difference between outflow and inflow was 2.22 C. On the high setting, this difference was 3.03 C. The heat carried by the water, per unit sensor plate area is $C = F\, c_w\, \Delta T/A$, where F is the flow rate of water (220 g/60 s), c_w is the specific heat of water (4.18 J g^{-1} C^{-1}), ΔT is the temperature difference, and A is the plate area (9×10^{-4} m^2). The convective loss was therefore 37.8 kW/m^2 on the low setting and 51.6 kW/m^2 on the high.

The average plate temperature, during these measurements was 27 C. If we assume the emissivity and absorptivity of the black plate to be 0.95, then, using the Stefan-Boltzmann law, the emitted flux density is 0.44 kW/m^2.

The radiant flux incident on the senor plate, H, can be computed from an energy balance. Neglecting conduction to the air, and radiation from the bottom of the sensor plate (because of its low emissivity), the energy balance is

$$a\,H - L - C = 0 \qquad (1)$$

where a is the absorptivity of the plate, and L is the emitted flux density. Solving for H gives:

$$H = (C + L)/a \quad . \qquad (2)$$

The values of H, for the high and low settings, were 54.8 and 40.3 kW/m^2. Taking an absorptivity for the soil surface as 0.75 gives absorbed radiation values of 41 and 30 kW/m^2.

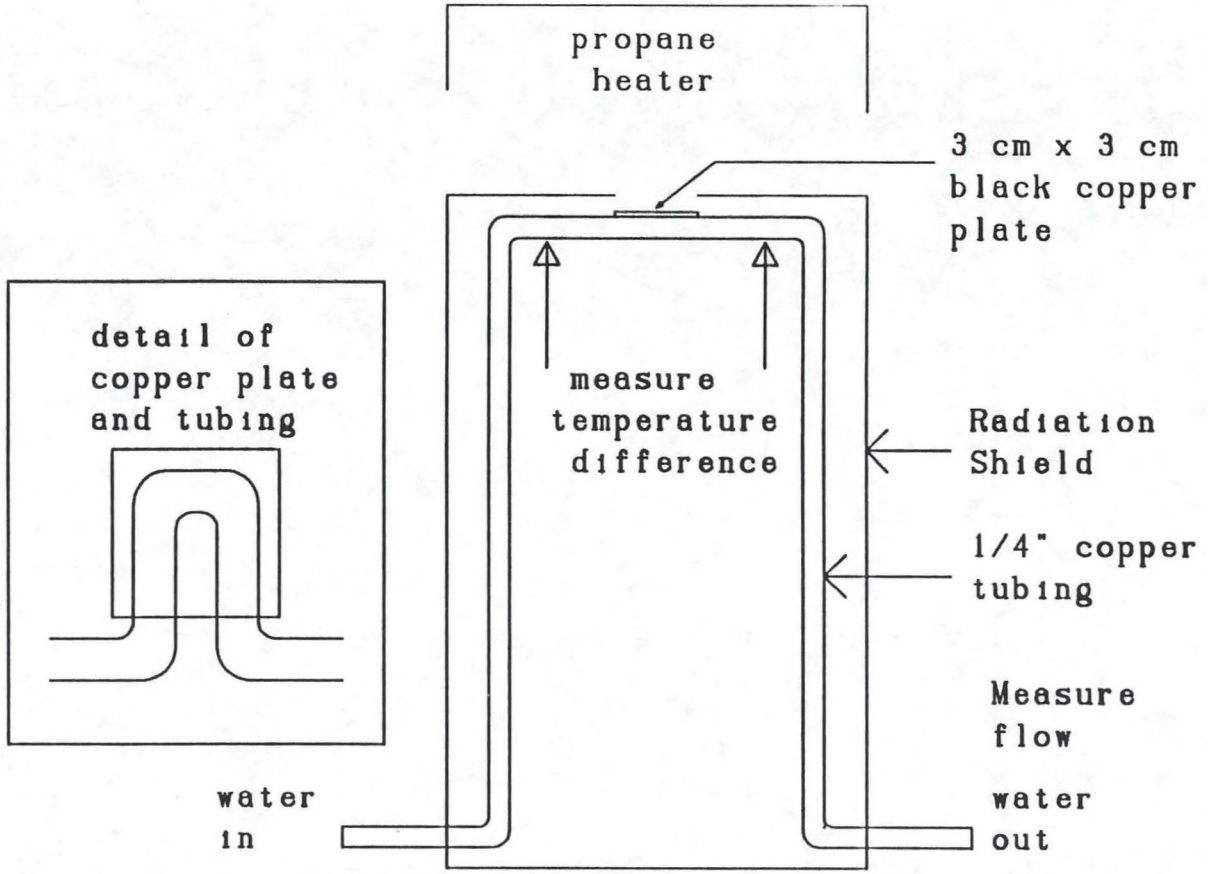

Figure 1. Diagram of radiometer and heater.

A Ventilated Psychrometer for Measuring the Vapor Pressure Under Fire

G. S. Campbell

Introduction

One of the critical boundary conditions needed for simulation of soil heating under fires is the vapor pressure near the soil surface. Water vapor in this space is contributed both by the burning of organic materials and by drying of the soil. Since temperatures are high, the vapor pressures can be well above the saturation vapor pressure in the atmosphere, making their measurement by gas sampling very difficult.

We simulated soil heating under a fire with a laboratory column, heated at the surface by a propane burner. In order to compare modeled soil temperatures with temperatures measured in the heated column, we needed vapor pressure measurements over the column. This paper describes a psychrometer that we built and used to make those measurements.

Psychrometer Design

The main features of the psychrometer are shown in Fig. 1. Air is drawn through a 1/2″ diameter x 10″ long stainless steel tube from under the fire. The air flows past a dry and a wet thermocouple, through a condenser, to remove excess water, and then to a small, rotary blower (Spiral Exhauster, model SE2A-1, Rotron, Inc, Woodstock, NY). The water reservoir is a 3″ diameter x 3-1/2″ high wide mouth jar with a plastic lid. The plexiglas assembly which holds the stainless steel tubing and the thermocouples is bolted to the lid of the jar. Holes were drilled through the lid for the wick and thermocouples. The plexiglas assembly was made from two pieces of 1/2″ thick plexiglas, each 1″ wide and 2.7″ long. These were clamped together, and a 1/2″ hole drilled axially for the thermocouple chamber, and to hold the stainless steel tube and the exit pipe. The bottom piece was then assembled to the lid, the thermocouples and wick were threaded through the holes, the thermocouples were positioned in the center of the thermocouple chamber, and the wick was threaded over the wet thermocouple and tied securely. The wick is a white, cotton shoelace which had been boiled to remove the sizing. The junction of the dry thermocouple was placed about 1″ upstream of the forward end of the wick to prevent interference of the wet with the dry temperature.

Thermocouples are chromel-constantan to minimize heat conduction along the wires. Once the thermocouples were in place, the top plexiglas piece was bolted into place, clamping the stainless steel tubing between the two pieces.

Operation

The psychrometer was placed so that the stainless steel tube would draw air from just above the soil surface, about 3 cm in from the edge. The flow of air through the psychrometer was adjusted by a clamp on the Tygon tubing leading to the rotary blower. We adjusted it to an air flow that appeared to just give full wet bulb depression. Even after minimizing the air flow, the dry temperature still ran above 350 C, and the wet bulb around 65 C. These high temperatures tended to melt the plexiglas, so it was necessary to wrap the back end of the stainless steel tube and the plexiglas assembly with paper toweling which we kept wet during runs. With this precaution, the psychrometer appeared to operate satisfactorily.

One difficulty with the psychrometer is the determination of the psychrometer constant for such high temperatures. We computed vapor pressures from the equation:

$$e_a = e_w^* - \gamma(T_a - T_w)$$

where e_a and e_w^* are the vapor pressure of air and the saturation vapor pressure at wet bulb temperature (T_w), and γ is the psychrometer constant. Gamma is normally computed from the product, AP, where P is atmospheric pressure. Tanner (1985) derived the temperature and vapor pressure dependence of A, showing that

$A(T_w,e_m) = [1+0.0016(T_w-20)][1-0.011(e_m - 2)]\ A(20,2)$,

where $e_m = (e_w+e_a)/2$. Tanner gives a value for A(20,2) of 0.00061 C^{-1}. At Pullman, P = 93 kPa. When $T_w = 65$, $e_w^* = 25$ kPa. Ambient vapor pressure is about 15 kPa, so $e_m = 20$ kPa. This gives A(65,20) = 1.07x0.80x0.00061 = 0.00052 C^{-1}. The psychrometer constant is therefore 0.00052x93 =0.0488 kPa/C. This was the value used for the reduction of the psychrometer data.

Results

Vapor pressure was measured during several heating experiments with a soil column under a propane burner (details of the heating experiments are given elsewhere in this report). Figure 2 shows a typical response of vapor

pressure, as measured by the psychrometer, over time for an initially wet soil column. The atmospheric vapor pressure is around 1 kPa. At about 10 min, the burner was lighted. The vapor pressure quickly increased to about 16 kPa, and then gradually decreased to between 13 and 14 kPa. Apparently the vapor from the propane burner was the main source of water vapor in this experiment. The drying of the soil surface did affect the vapor concentration, but only by 10 to 15% of the total change.

Summary

A ventilated psychrometer appeared to give reasonable estimates of vapor pressure above a soil surface being heated by a propane burner. Water vapor from the combustion of the propane appeared to be the most important factor in determining the vapor pressure at the surface of the soil, with evaporation from the soil making a much smaller contribution.

Reference

Tanner, C. B. 1985. The psychrometer constant. Unpublished notes, Dept. of Soil Science, University of Wisconsin, Madison, WI 68583.

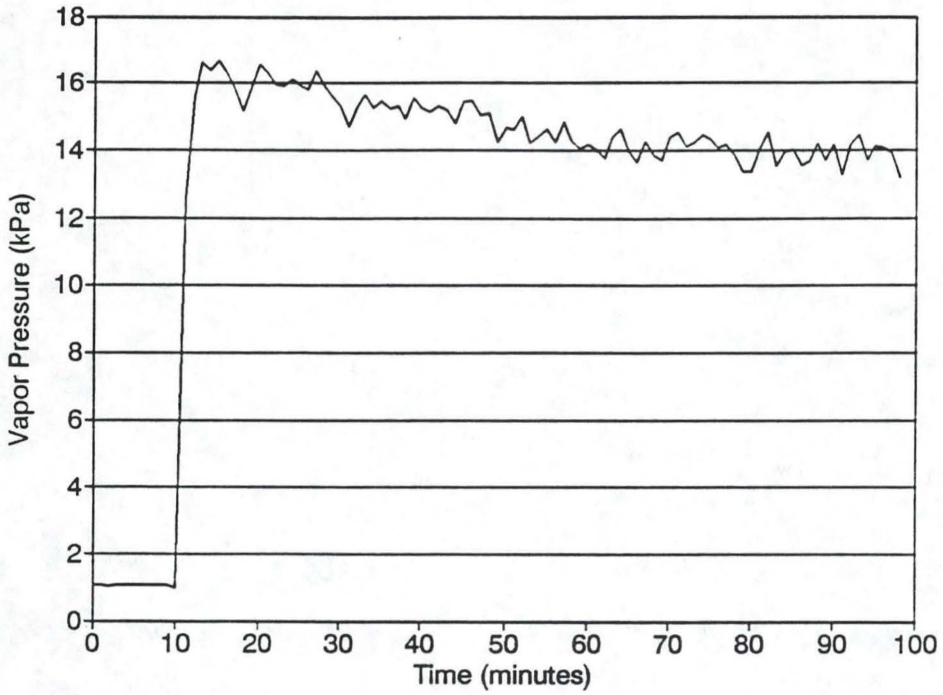

Figure 2. Vapor pressure as a function of time over a heated soil column. The fire was started at 10 min. The decrease in vapor pressure with time is probably the result of soil drying at the surface.

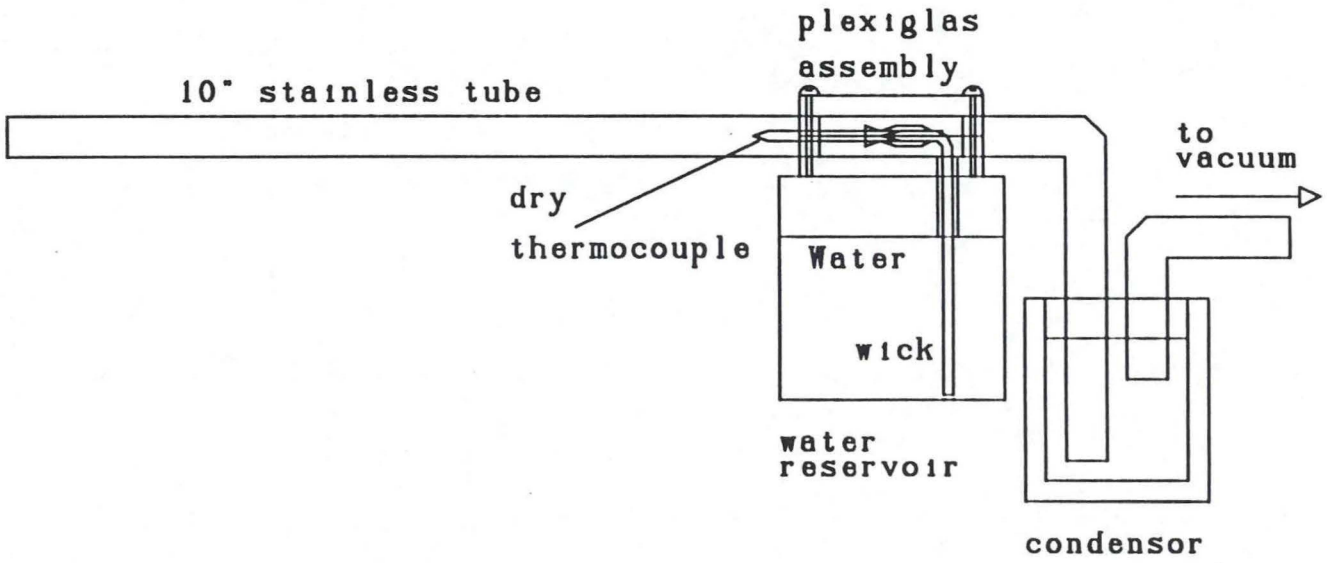

Figure 1. Diagram of Psychrometer